



Norwegian University of
Science and Technology

Next Generation Design of Satellite Brackets

By Using Topology Optimization and Additive
Manufacturing

Øyvind Sanden

Master of Science in Mechanical Engineering

Submission date: June 2018

Supervisor: Jan Torgersen, MTP

Co-supervisor: Filippo Berto, MTP

Norwegian University of Science and Technology
Department of Mechanical and Industrial Engineering

Abstract

This thesis has explored how topology optimization and additive manufacturing can be used to improve the resonance performance of existing mechanical components. By using a sensitivity-based optimization algorithm for minimum compliance, the resulting optimized components show an increased natural frequency compared to the original components. Three brackets holding the payload of the AISSat 1 satellite were used as baseline components. Two different design optimizations were performed. In the first result, each bracket was optimized individually, while the second result combined the three brackets into one component. The natural frequency of the original center bracket was increased from 3224 Hz to 3849 Hz and the top and bottom brackets increased from 2667 Hz to 4138 Hz. The one-piece bracket achieved a natural frequency of 3795 Hz. A weight target of 36 grams based on the total weight of the original brackets was used. This target was not met by either result. The individual brackets amassed to a total of 43.4 grams, while the one-piece bracket weighed 39.9 grams.

Sammen drag

Denne oppgaven har undersøkt hvordan topologi optimalisering og additiv tilvirking kan brukes til å forbedre resonansytelsen til eksisterende mekaniske komponenter. Ved å bruke en sensitivitetsbasert optimaliseringsalgoritme for minimum komplians, viser de resulterende optimaliserte komponentene en økt egenfrekvens sammenlignet med de originale komponentene. Tre braketter som holder nyttelasten til AISSat 1-satellitten ble brukt til sammenligning. To forskjellige designoptimeringer ble utført. I det første resultatet ble hver brakett optimalisert individuelt, mens i det andre resultatet ble de tre brakettene kombinert til én komponent. Egenfrekvensen til den opprinnelige senterbraketten økte fra 3224 Hz til 3849 Hz, og topp- og bunnbebrakettene økte fra 2667 Hz til 4138 Hz. Den sammenhengende braketten oppnådde en egenfrekvens på 3795 Hz. Et vekt mål på 36 gram ble brukt, basert på totalvekten til de originale komponentene. Dette målet ble ikke oppfylt av noen av resultatene. De individuelle brakettene fikk en samlet vekt på 43,4 gram, mens den sammenhengende braketten veide 39,9 gram.

Preface

This Master's thesis has been submitted to the Norwegian University of Science and Technology (NTNU) during the spring semester of 2018. The thesis was carried out at the Department of Mechanical and Industrial Engineering (MTP) under the supervision of Associate Professor Jan Torgersen and co-supervisor Filippo Berto. The work was done in cooperation with the Norwegian Defence Research Establishment (FFI).

Acknowledgment

I would like to thank Jan Torgersen and Filippo Berto for the guidance and motivation throughout the project, as well as the opportunity to write about such an exciting topic. Also, thanks to Bendik Sagsveen at FFI for providing an interesting problem and valuable discussions during the project. I would also like to thank fellow students Thomas Herstad and Brage Vasseljen for their help on the setup in Abaqus and Tosca, and Stig Strømsnes for general engineering advise.

Contents

Abstract	i
Sammendrag	iii
Preface	v
Acknowledgment	vii
Contents	viii
List of Figures	x
List of Tables	xii
1 Introduction	1
1.1 Problem Definition	1
1.2 AISSat 1	2
1.3 Topology Optimization	2
1.3.1 Sensitivity-Based and Condition-Based Algorithms	3
1.4 Additive Manufacturing	4
1.4.1 Mechanical Properties	5
1.4.2 STL File	6
1.4.3 Slicing	7
1.4.4 Design for Space	8
2 Theory	9
2.1 Topology Optimization Theory	9
2.1.1 Minimum Compliance Design	9
2.1.2 Material Model	10
2.1.3 Solution Method	11
2.2 Natural Frequencies	13
3 Method	15
3.1 Problem Setup	15
3.1.1 Design Space	15
3.1.2 Loads	16
3.1.3 Materials	20
3.1.4 Analysis Setup	20
3.1.5 Optimization Setup	22
3.1.6 Frequency Analysis	22
3.2 Post-processing	23

4	Results	27
4.1	Optimization Results	27
4.2	Stresses and Strains	30
4.3	Natural Frequencies	31
4.4	Manufacturing	33
5	Discussion	35
5.1	Problem Setup	35
5.2	Results	38
5.3	Post-Processing	40
6	Conclusion	43
6.1	Future Work	43
A	Abaqus Setup	47
A.1	Part	47
A.2	Properties	50
A.3	Assembly	52
A.4	Step	54
A.5	Interaction	56
A.6	Load	63
A.7	Mesh	65
	A.7.1 Bolts	65
	A.7.2 Design Space	66
A.8	Optimization	68
B	Post-Processing	71
C	Previous Models	81
D	Matlab Code	87
E	Arianespace Axuiliary Passengers User’s Manual	89
F	EOS Aluminum AlSi10Mg Data Sheet	97

List of Figures

1	Rendering of the satellite payload assembly.	1
2	Illustration of the AISSat 1 in space.	2
3	Sizing, shape and topology optimization.	3
4	Condition-based and sensitivity-based algorithms.	4
5	Tensile properties of Ti6Al4V with different AM processes.	7
6	Staircase effect.	8
7	Normal modes for a simply supported beam or axle	13
8	Natural frequencies as a function of diameter and length.	14
9	Side view of the payload assembly.	15
10	The design spaces used for the two cases.	16
11	Dimensions for the design space.	16
12	Usable volume for auxiliary passengers.	18
13	Interactions in Abaqus.	21
14	Boundary condition during the frequency analysis.	22
15	The effect of smoothing cycles.	24
16	Render of the finished one-piece bracket.	25
17	Render of the finished center bracket.	25
18	Render of the finished top and bottom brackets.	26
19	Before and after post-processing of the one-piece bracket.	26
20	Optimization results of the one-piece bracket.	27
21	Optimization results of the individual brackets.	28
22	Plot of the design cycles for the one-piece bracket.	28
23	Plot of the design cycles for the individual brackets.	29
24	Von Mises stresses after combination.	30
25	Strains after combination.	30
26	Different optimized print orientations.	33
27	Support areas for different orientations.	34
28	The effect of an extended design space.	35
29	Tilted view of the one-piece bracket in Abaqus.	38
30	Mesh on the new center bracket.	41
A.1	Import dialogue box.	48
A.2	Parts used in Abaqus.	49
A.3	Overview of units relations in Abaqus.	50
A.4	Properties used for AlSi10Mg.	50
A.5	Properties used for steel.	51
A.6	Material orientation.	51
A.7	Create instance.	52
A.8	Rear view of the assembly.	53
A.9	Create linear perturbation step.	54
A.10	Step manager.	55
A.11	Find contact pairs.	57
A.12	Interaction manager.	58
A.13	Interactions with master and slave surfaces.	59

A.14 Contact properties.	60
A.15 Tie between the countersunk bolts and the design space.	60
A.16 Creating the wire feature.	61
A.17 Connector section creation and assignment.	61
A.18 Diagram of the connector properties.	62
A.19 Bolt coupling.	62
A.20 Load case 1.	63
A.21 Load manager.	63
A.22 Boundary conditions.	64
A.23 Bolt mesh and sections.	65
A.24 Mesh controls used for the bolts.	65
A.25 Settings used for the bolt mesh.	66
A.26 Design space mesh.	67
A.27 Settings used for the design space mesh.	67
A.28 Optimization process workflow.	68
A.29 Design responses.	69
A.30 Objective function and constraint for the optimization.	70
A.31 Frozen areas.	70
B.32 STL file imported into Fusion 360.	71
B.33 Quarter of the mesh body.	72
B.34 Smooth edges because of the T-spline body.	73
B.35 Before and after smoothing.	73
B.36 Before and after smoothing.	74
B.37 Result after excessive smoothing.	74
B.38 Exporting to an OBJ file in ReCap.	75
B.39 Converting from mesh to a T-spline body.	75
B.40 Converted T-spline body.	76
B.41 The handle used to edit the T-spline body.	76
B.42 Before and after editing the the top edge of the T-spline body.	77
B.43 The difference between the T-spline body and mesh body	77
B.44 Converting from a T-spline body to a solid body.	78
B.45 Converted to a solid body.	78
B.46 The finished body in NX.	79
C.47 Full satellite assembly with the top and side panels removed.	81
C.48 Symmetric satellite assembly.	82
C.49 Load applied to the satellite assembly.	83
C.50 The complete design space before it was made symmetric.	84
C.51 Front and rear view of the results with titanium.	84
C.52 Result after 22 cycles.	85
C.53 Quarter model.	85

List of Tables

1	Mechanical properties of AlSi10Mg after heat treatment.	6
2	Design load cases.	17
3	Load cases.	18
4	Calculated values for the load cases.	19
5	Material properties for AlSi10Mg.	20
6	Natural frequencies and weight of the center brackets	31
7	Natural frequencies and weight of the top and bottom brackets	32
8	The natural frequencies and weight of the one-piece bracket.	32
9	Support info for the two orientations.	33

1 Introduction

1.1 Problem Definition

This project is designed as a feasibility study in association with the Norwegian Defence Research Establishment (FFI) to look at how topology optimization and additive manufacturing can be used to improve the resonance performance of mechanical components. Three brackets from the existing AISSat 1 satellite will be used as benchmark components for the stiffness, measured by the natural frequencies. These are the black components on both sides of the payload assembly in figure 1. The objective is stiffness and eigenfrequency optimization of the satellite brackets using topology optimization. Two scenarios will be explored: one where a single component is used, and one where the individual brackets are optimized separately. The natural frequencies of the components will then be compared. The optimization will be limited to quasi-static loads. The software used for the optimization will be Abaqus 2017 and Tosca Structure. The problem setup and finite element analysis will be done in Abaqus, while the calculations for the optimization process are done in Tosca. The optimized parts will be based on the geometric constraints of the original brackets.



Figure 1: Rendering of the satellite payload assembly.

1.2 AISSat 1

The AISSat 1 is a satellite designed to monitor the Automatic Identification System (AIS) signals from maritime vessels in the oceans under Norwegian jurisdiction. The satellite was launched in 2010. Ships over 300 gross tonnes are required to have an AIS on board that transmits information such as the position, course, and speed of the ship [1]. Monitoring these signals can be used for ship traffic surveillance and to identify potential illegal fishing. The information gathered can also be used in rescue missions [2].

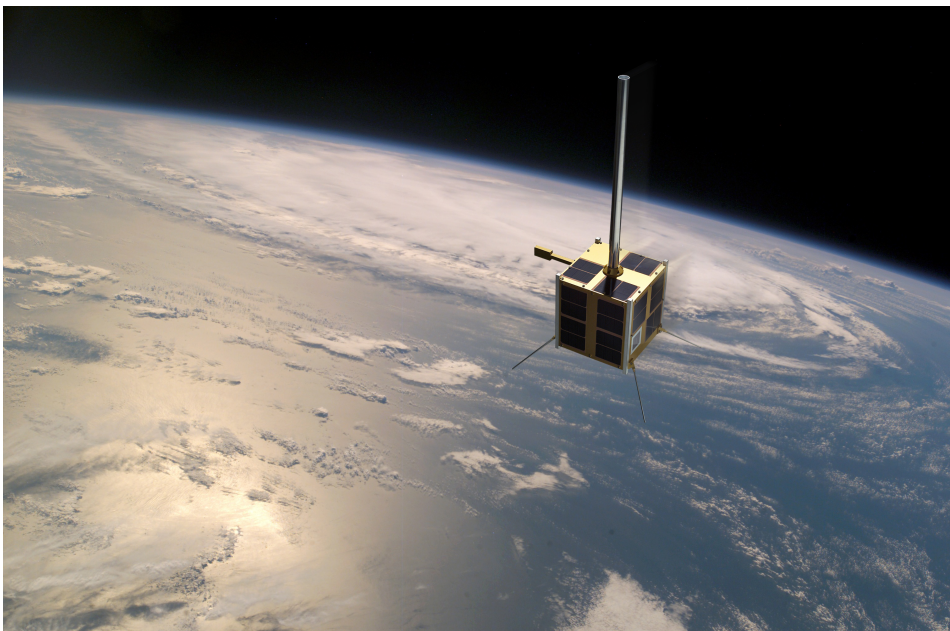


Figure 2: Illustration of the AISSat 1 in space [3].

The satellite is built based on the Generic Nanosatellite Bus (GNB), with a total mass of 6 kg. The main structure is a cube with sides measuring 200 mm.

1.3 Topology Optimization

The goal of topology optimization is to find the optimal distribution of material within a given region based on a given volume fraction, loads, supports and other possible design restrictions, such as holes or solid areas. Structures can be optimized for several problems, for example, maximum stiffness or maximum buckling loads. One of the most typical uses of topology optimization is a minimum compliance design, which is equivalent to maximizing the global stiffness in a structure. In

this problem, strain energy is usually used as a design response, and the objective function is to minimize this response.

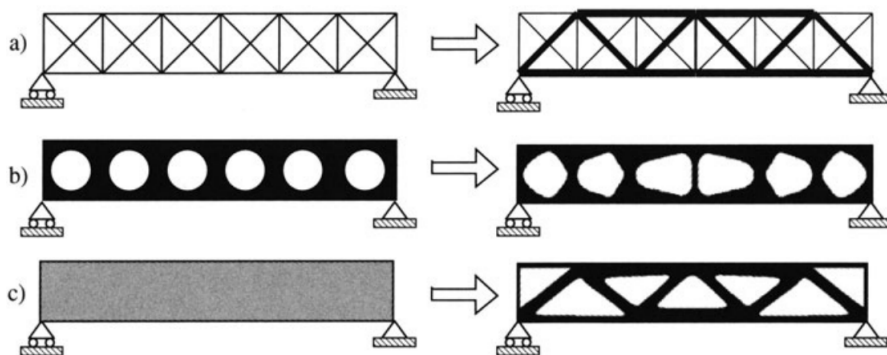


Figure 3: Different categories of optimization. a) Sizing optimization, b) shape optimization, c) topology optimization [4].

In addition to topology optimization, sizing and shape optimization are other forms of structural design problems. Sizing optimization is typically used to find the optimal sizing of a design variable, such as thickness or cross-section area of a truss. For shape optimization, the shape of the structure is allowed to change. The problem is to find the optimal shape of the domain, for example by changing the position of the nodes that define the boundary of the structure. Topology optimization takes this a step further. This optimization allows the creation of holes, as well as the size, location, and shape of these holes. Illustrations of the different optimization processes can be seen in figure 3 [4, 5].

1.3.1 Sensitivity-Based and Condition-Based Algorithms

Abaqus/Tosca offers two different optimization algorithms, sensitivity-based or condition-based. The sensitivity-based optimization can utilize two different material interpolation techniques, SIMP (Solid Isotropic Material with Penalization) or RAMP (Rational Approximation of Material properties). A comparison between the results from the two algorithms for a minimum compliance problem can be seen in figure 4. The main difference between the algorithms is that the condition-based method starts with the complete design space and removes material during the iterations, while the sensitivity-based method starts with only the frozen areas and then adds material. In the final result, the sensitivity-based algorithm produces generally larger members than the condition-based one. This is something that can affect the need for support structure if the parts are manufactured using additive manufacturing (AM).

Another difference between the methods is that the condition-based is generally

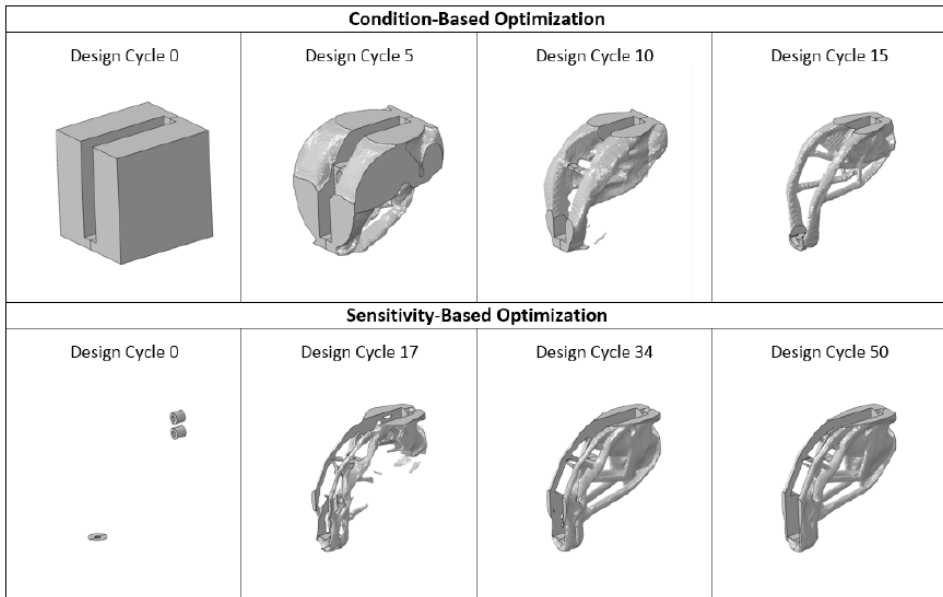


Figure 4: Design iterations using condition-based and sensitivity-based algorithms [6].

more effective in terms of the number of iterations needed. However, it can only be used for a minimum compliance problem as the only available design responses are strain energy and volume. While the sensitivity-based method generally requires more iterations, it is capable of solving more complex problems with multiple constraints and objectives. The number of available design responses is also higher. In addition to volume and strain energy, weight, displacement, rotation, stress, eigenfrequency, center of gravity, and moment of inertia among others can be used as design responses [6].

1.4 Additive Manufacturing

Additive manufacturing, commonly known as 3D printing, has opened doors in manufacturing that was never thought possible a couple of decades ago. Complex components that previously needed hours of extensive machining are now possible to manufacture directly from a 3D model. AM has over the last decades gone from being an ultra high-tech and expensive tool to a household item for the fanatics of modern technology.

AM is a manufacturing process that, instead of removing material to reveal the product, builds it up layer by layer. This is a process that in many cases removes

the need for both processes in forming and joining. The importance and flexibility of AM have been realized by different industries, which has inspired more research in the field. This research has again exposed further possibilities when it comes to both usable materials and manufacturing techniques [7].

The process allows engineers and designers to go directly from a Computer-Aided Design (CAD) model to physical products without the need for special tooling. More complex geometries, saving time and money, as well as earlier customer involvement, are some of the possible advantages of additive manufacturing. Common drawbacks and challenges include poor surface quality and physical properties [8]. However, each AM technology has its own set of advantages and disadvantages, in addition to a limited material selection.

Different additive manufacturing processes can be distinguished according to the heat source and how the material is deposited. Different heat sources include laser, electron beam, and arc welding. Powder or wire feeding are common methods for material deposition. The main categories of technologies are powder bed fusion (PBF) and directed energy deposition (DED). The basic function of powder bed fusion is that powder is spread in layers and then solidified by a heat source to generate a solid shape. Processes such as electron beam melting (EBM), selective laser melting, (SLM) and direct metal laser sintering (DMLS) are examples of powder bed fusion technologies. The main difference between these methods is the heat source, and how this is applied to the powder. In contrast, directed energy deposition is based on material that is deposited directly into the power source. DED includes technologies like laser-engineered net shaping (LENS), direct metal deposition (DMD) and wire and arc additive manufacturing (WAAM) [9].

1.4.1 Mechanical Properties

One of the major challenges with additive manufactured parts are the anisotropic properties. Because of this, the parts can change the behavior depending on the orientation during manufacturing. An example of this can be seen in table 1 which shows the properties of AlSi10Mg, a material used in DMLS machines, after heat treatment. Although this is not highly anisotropic, it can still be challenging for engineers to work the material. After the DMLS process, the density of the material will be approximately 99.85 %. The complete datasheet can be seen in Appendix F.

A lot of the research on mechanical properties of additive manufactured parts have been done on titanium alloys. An overview of tensile properties of various AM processes using Ti6Al4V can be seen in figure 5. From this figure, it can be seen that the strength from all the additive methods equals or surpasses the cast, forged, and wrought properties. The opposite is true for the ductility. The differences in thermal cycles between the processes will lead to differences in the microstructure

Tensile Strength	
- in horizontal direction	345 ± 10 MPa
- in vertical direction	350 ± 10 MPa
Yield Strength	
- in horizontal direction	230 ± 15 MPa
- in vertical direction	230 ± 15 MPa
Young's Modulus	
- in horizontal direction	70 ± 10 GPa
- in vertical direction	60 ± 10 GPa
Elongation at Break	
- in horizontal direction	12 ± 2%
- in vertical direction	11 ± 2%

Table 1: Mechanical properties of AlSi10Mg after heat treatment. Reconstructed from Appendix F.

of the material. By using heat treatment, the features of the microstructure can be altered, and defects and residual stresses can be reduced, or even eliminated [9].

Even though AM parts have shown good tensile properties, the fatigue properties can be a major concern. AM parts often suffer from a high surface roughness, which can provide stress concentrations which can affect the fatigue life of the parts. Studies have shown that reducing the surface roughness by machining and polishing can increase the fatigue limit. For 316L stainless steel, the fatigue limit was increased from 200 MPa in the as-built condition to 260 MPa after machining and polishing [10]. The porosity of the parts can lead to internal defects that also impact the fatigue life. It has been reported that heat treatment can also increase the fatigue strength. A combination of heat treatment and surface machining will lead to the best results in terms of fatigue by almost eliminating process-induced defects [9].

1.4.2 STL File

The STL file is a common and simple way to represent 3D geometry for processing in additive manufacturing. In this file format, 3D surfaces are defined by the coordinates of three vertices of a triangle in a three-dimensional space, along with the direction of the surface normal. Each triangle is represented separately from each other [11].

There are a number of problems with this formatting which can result in errors in the 3D model. Firstly, because each triangle is defined separately, rounding errors in the position of adjacent triangles can cause voids between the surfaces. Other

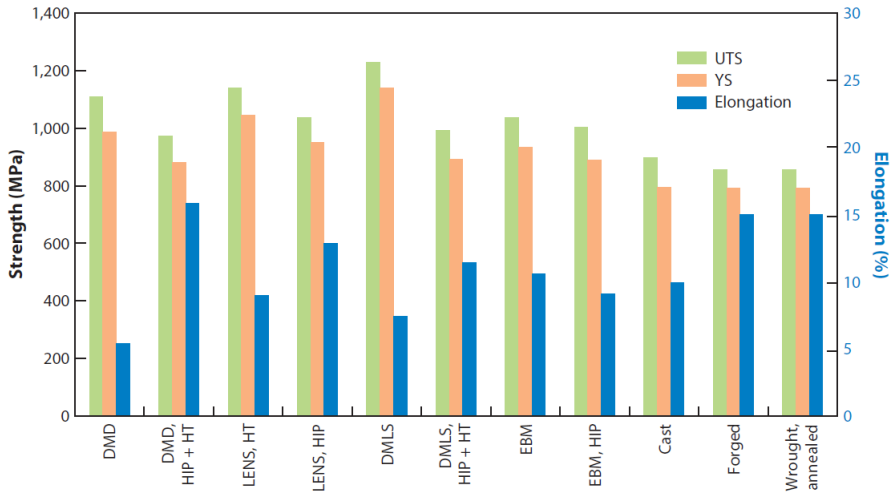


Figure 5: Tensile properties of Ti6Al4V with different AM processes. Abbreviations: UTS - ultimate tensile strength, YS - yield stress, HT - heat treated [9].

issues can be caused by an inverted surface normal. The file format is also lacking units, which can cause both engineering and manufacturing problems. Finally, a very common issue is the scalability of the files. Because only triangles are used to define surfaces, a very high number of triangles are needed to represent a complex geometry with good accuracy. This makes the file sizes excessively large because of the high number of data points [12].

1.4.3 Slicing

Before the path for each layer can be planned, the 3D model must first be divided into 2D layers. The most common practice is to convert the 3D geometry into an STL file which is then sliced into layers from the bottom to the top with a certain layer thickness.

For curvature based areas, smaller layer thicknesses will give better accuracy [13]. Similarly, a thicker layer will result in a larger dimensional error. This is due to a common problem experienced with AM called the staircase effect, illustrated in figure 6. The dashed line indicates the original curvature of the model. In this case, the top edge of the layers is coincident with the boundary of the CAD model. This leaves an area between the boundary of the layered part and the model without material.

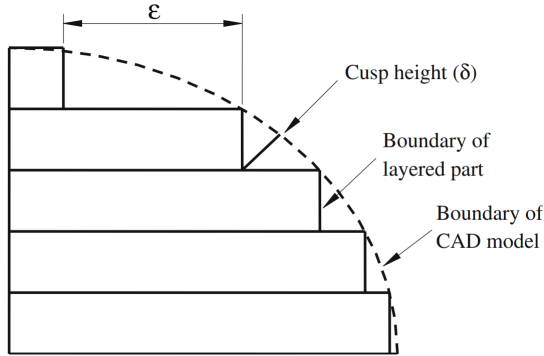


Figure 6: Staircase effect due to the layered build-up [13].

1.4.4 Design for Space

The space industry is an industry that faces very difficult technical challenges. Launch costs are extremely high, and there are little to no opportunities for repair after launch. Because of this, there are strict design requirements in this industry. This creates some challenges when using additive manufacturing. Questions regarding the material data and verification of the performance of the manufactured components are important to answer. For space products, the extreme environments they operate in and the requirements of the system around the components will be driving factors for the design. In this market, long development cycles are common, along with long life cycles and low volumes of components.

While additive manufacturing is generally thought of as an expensive process, the low volumes can help balance the cost compared to traditional manufacturing processes. Firstly, no special tools are needed for the different components. This reduces the time and cost related to the potential tools. The generation of the machine code for AM is also easier and faster than for subtractive processes because of the more automatic slicing programs. This helps to reduce the non-recurring costs. AM is also associated with less waste than traditional manufacturing. Scrap material is reduced, and there is no need for cutting fluids. With larger machines, it is also possible to run multiple manufacturing jobs at one [14].

2 Theory

2.1 Topology Optimization Theory

2.1.1 Minimum Compliance Design

The following sections (2.1.1 and 2.1.2) will describe the problem setup of a minimum compliance problem with an isotropic material, gathered from Bendsøe and Sigmund (2004) [4]. The problem can be defined as finding the optimal stiffness tensor $E_{ijkl}(x)$ over the design domain Ω . By using the energy bilinear form

$$a(u, v) = \int_{\Omega} E_{ijkl}(x) \epsilon_{ik}(u) \epsilon_{kl}(v) \, d\Omega \quad (1)$$

along with linearized strains $\epsilon_{ij}(u) = \frac{1}{2} \left(\frac{\delta u_i}{\delta x_j} + \frac{\delta u_j}{\delta x_i} \right)$ and the load in linear form

$$l(u) = \int_{\Omega} f u \, d\Omega + \int_{\Gamma_T} t u \, ds, \quad (2)$$

gives the minimum compliance problem the form of:

$$\begin{aligned} & \min_{u \in U, E} l(u) \\ \text{subject to: } & a_E(u, v) = l(u), \quad \text{for all } v \in U, \\ & E \in \mathbf{E}_{\text{ad}} \end{aligned} \quad (3)$$

Here, U are the kinematically admissible displacement fields, f are the body forces, t is the boundary condition on the traction part $\Gamma_T \subset \Gamma \equiv \partial\Omega$ and \mathbf{E}_{ad} is the set of admissible stiffness tensors for the problem. The equilibrium is written in its weak, variational form. Both the stiffness E and displacement u are fields of interest in equation (3). By discretizing E as constant in each element and using the same finite element (FE) mesh for both fields, the discrete form of the compliance problem can be written as:

$$\begin{aligned} & \min_{u \in U, E} \mathbf{f}^T \mathbf{u} \\ \text{subject to: } & \mathbf{K}(E_e) \mathbf{u} = \mathbf{f} \\ & E \in \mathbf{E}_{\text{ad}} \end{aligned} \quad (4)$$

where \mathbf{u} is the displacement vector, \mathbf{f} is the load vector and \mathbf{K} is the stiffness matrix dependent on the stiffness of each element.

In the optimization, we are interested in the optimal distribution of isotropic material in space. Any given point will either be occupied by material or a void. In the reference domain Ω , the material points will be part of the subset Ω^{mat} . With this, the set of admissible stiffness tensors \mathbf{E}_{ad} can be written as:

$$E_{ijkl} = 1_{\Omega^{\text{mat}}} E_{ijkl}^0, \quad 1_{\Omega^{\text{mat}}} = \begin{cases} 1, & \text{if } x \in \Omega^{\text{mat}}, \\ 0, & \text{if } x \in \Omega \setminus \Omega^{\text{mat}}, \end{cases} \quad (5)$$

$$\int_{\Omega} 1_{\Omega^{\text{mat}}} \, d\Omega = \text{Vol}(\Omega^{\text{mat}}) \leq V.$$

V determines the amount of available material. E_{ijkl}^0 is the isotropic stiffness tensor for the material used. The problem is now a discrete-valued design problem with values either 0 or 1. To solve this problem, the integers can be replaced with continuous variables. The optimization must result in areas of either material or voids which means that the continuous variable must be penalized towards the discrete values. This will remove artificial densities in the design. The SIMP model can be used for this. This model can be written as:

$$E_{ijkl}(x) = \rho(x)^p E_{ijkl}^0, \quad p \geq 1, \quad (6)$$

$$\int_{\Omega} \rho(x) \, d\Omega \leq V; \quad 0 \leq \rho(x) \leq 1, \quad x \in \Omega,$$

$$E_{ijkl}(\rho = 0) = 0, \quad E_{ijkl}(\rho = 1) = E_{ijkl}^0, \quad (7)$$

This means that if the final design is strictly made of densities of either 1 or 0, the result will be a “black-and-white” design. Values of $p > 1$ are chosen. This makes the stiffness gained by intermediate densities small compared the cost of the material. A typical value used is $p = 3$ [15].

2.1.2 Material Model

SIMP can be considered a material model if:

$$p \geq \max \left\{ \frac{2}{1 - \nu^0}, \frac{4}{1 + \nu^0} \right\} \quad (\text{in 2D}) \quad (8)$$

$$p \geq \max \left\{ 15 \frac{1 - \nu^0}{7 - 5\nu^0}, \frac{3}{2} \frac{1 - \nu^0}{1 - 2\nu^0} \right\} \quad (\text{in 3D}) \quad (9)$$

Here, ν^0 is Poisson's ratio for the material. According to equation (9), aluminum with $\nu = 0.33$ should use $p \geq 2.96$ for SIMP to be considered a material model in 3D. The typical value of $p = 3$ is therefore an acceptable choice.

2.1.3 Solution Method

To solve the optimization problem, an iterative solving method will be used. This method must be able to update the design variables at each point separately from the other points, based on the optimality conditions and the previously computed design and its displacements. For this, equation 3 will be rewritten as [4]:

$$\begin{aligned}
 & \min_{u \in U, E} l(u) \\
 \text{subject to: } & a_E(u, v) = l(u), \quad \text{for all } v \in U, \\
 & E_{ijkl}(x) = \rho(x)^p E_{ijkl}^0, \\
 & \int_{\Omega} \rho(x) \, d\Omega \leq V; \quad 0 < \rho_{min} \leq \rho \leq 1.
 \end{aligned} \tag{10}$$

The procedure to solve this optimization problem and find the optimal topology for a given structure with an isotropic material is as follows:

Pre-Processing

1. Select an appropriate design domain along with boundary conditions and loads.
2. Select regions in the design domain that will be fixed as solid or voids. These regions are known as frozen regions.
3. Generate a finite element mesh. The resolution of the mesh should be fine enough to accurately represent the design domain.
4. Make a homogeneous distribution of the material.

Optimization

From this point, an iterative algorithm will begin to work through the following procedure:

1. Use a finite element analysis (FEA) to compute the resulting strains and displacements of the design.

2. Compute the compliance. Stop the iterations if only a marginal improvement in compliance is achieved, or if the necessary conditions of optimality are satisfied. If not, continue.
3. Update the design variables. Add material to areas where the strain energy is below a given threshold, and remove material in areas with energy below this value. The equations for this limit are described in detail in section *1.2.1 Conditions of optimality* in Bendsøe and Sigmund (2004) [4]. The frozen areas are excluded from this step.
4. Restart the iteration loop.

Post-processing

The final step is to represent the result visually, for example as a body in a 3D space. This result can be further post-processed by filtering, smoothing and a final CAD regeneration of the structure. The result from the topology optimization is typically in the form of a mesh body in an STL file. There are typically two approaches to post-processing:

1. Full CAD reconstruction where all the features of the model are recreated by solid modeling, surface modeling, sculpting or a combination of these techniques.
2. Mesh manipulation by smoothing and filtering operations.

Many CAD programs have features for reverse engineering, as this is something that is increasingly in demand. Reverse engineering tools are not just important for topology optimization results, but also for 3D scanning. With these features, the software can typically recognize the surfaces of the mesh body. Examples of this are sketches that can be made directly from these surfaces. If sculpting is used, the control points of the sculpted body can be moved automatically to the surface of the mesh. There is, however, no fully automatic method to go from an optimization result to a finished part ready for manufacturing.

2.2 Natural Frequencies

The natural frequency of a component is defined as the lowest inherent rate of free vibration of the component vibrating between its own ends [16]. A general form for the natural frequency ω_e is:

$$\omega_e = \sqrt{\frac{k}{m}} \quad (11)$$

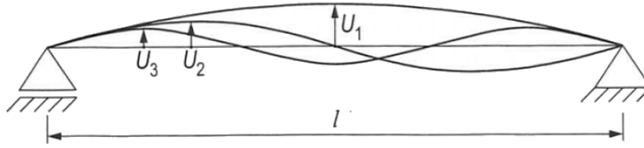


Figure 7: Normal modes 1-3 for a simply supported beam or axle [17].

Slim members can become an issue for topology optimized parts when a certain minimum natural frequency is desired. This problem can be simplified to a simply supported prismatic beam or axle, as seen in figure 7, with bending modes parallel to one of the cross section's principal axes. The equation for the n th natural frequency mode ω_{en} can be written as [17]:

$$\omega_{en} = \frac{n^2 \pi^2}{l^2} \sqrt{\frac{EI}{\rho A}} \quad (12)$$

Here, l is the length, A the area of the cross-section, ρ the material density, E is Young's modulus and I is the second moment of area. By looking at the first mode of a solid cylindrical axle, $n = 1$, with $A = \frac{\pi}{4} d^2$ and $I = \frac{\pi}{64} d^4$, the equation can be rewritten as:

$$\omega_{e1} = \frac{\pi^2}{l^2} \sqrt{\frac{E(\frac{\pi}{64} d^4)}{\rho(\frac{\pi}{4} d^2)}} \quad (13)$$

$$\omega_{e1} = \frac{\pi^2 d}{l^2} \sqrt{\frac{E}{16\rho}} = \frac{\pi^2 d}{4l^2} \sqrt{\frac{E}{\rho}} \quad (14)$$

The unit for this equation is rad/s . By dividing by 2π , the unit is converted to Hertz:

$$\omega_{e1} = \frac{\pi d}{8l^2} \sqrt{\frac{E}{\rho}} \quad (15)$$

By using $\rho = 2700 \text{ kg/m}^3$ and $E = 70 \text{ GPa}$, which are typical values for aluminum, the natural frequency can be plotted as a function of the diameter for different lengths:

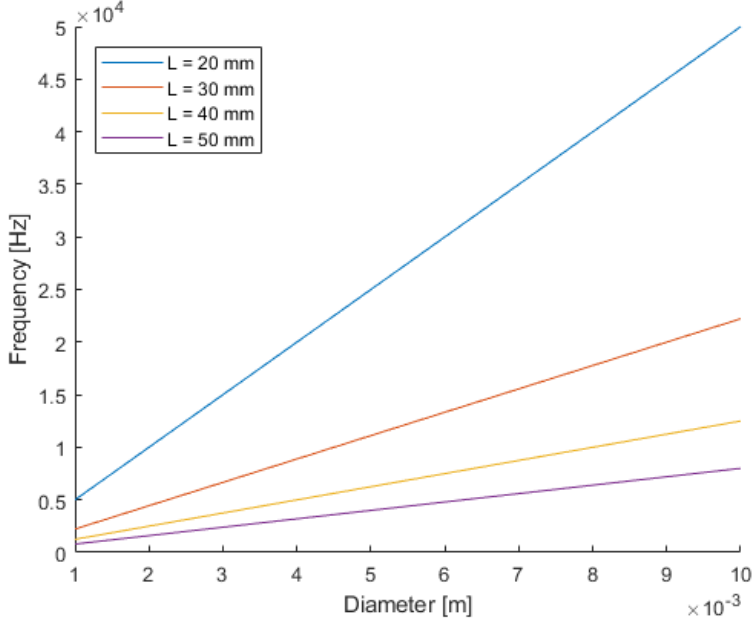


Figure 8: Natural frequencies as a function of diameter and length. See Appendix D for the code used to generate the plot.

This plot can be used to determine the minimum member size that can be used in an optimization process to ensure a certain natural frequency is achieved. The natural frequency of a highly organic structure can be difficult to predict using simple equations, but this could still be useful to set a baseline.

3 Method

3.1 Problem Setup

Everything for the problem setup for the two scenarios is equal, except for the design spaces.

3.1.1 Design Space

The design space for this problem is constrained by the size of the targeted brackets. For the one-piece problem, the combined volume encapsulated by the three brackets will be used. For the second problem, one design space will be defined based on each bracket.

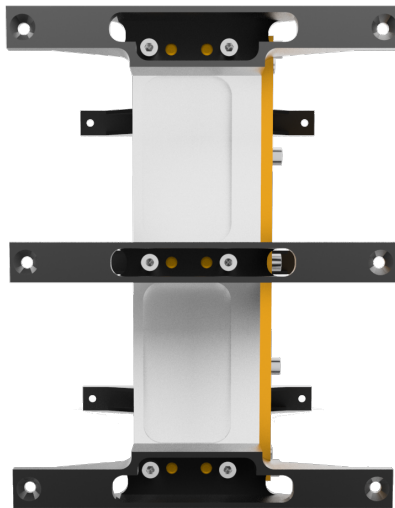


Figure 9: Side view of the payload assembly.

Due to the geometry of the satellite's payload and other conditions, the original parts were designed slightly unsymmetrical, as can be seen in figure 9. In order to simplify this problem, however, the distance between the outer and inner bolts have been adjusted in order to achieve symmetry. The open volume around the inner bolts has also been increased slightly so that a washer could be used during assembly. The design spaces used for the two cases can be seen in figure 10. The dimensions for the top view can be seen in figure 11. These dimensions were also slightly altered from the original parts to increase the design space. A small fillet

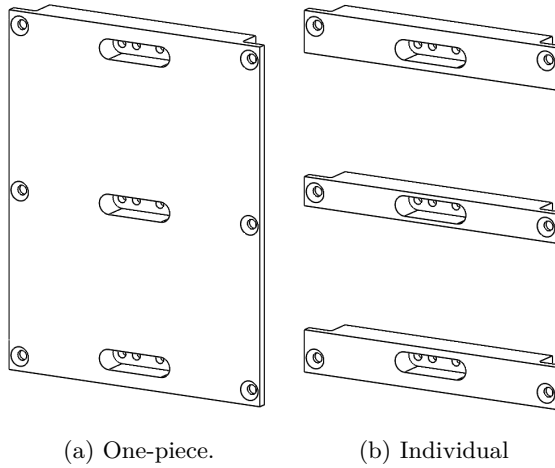


Figure 10: The design spaces used for the two cases.

was also added in order to prevent any stress concentrations from forming.

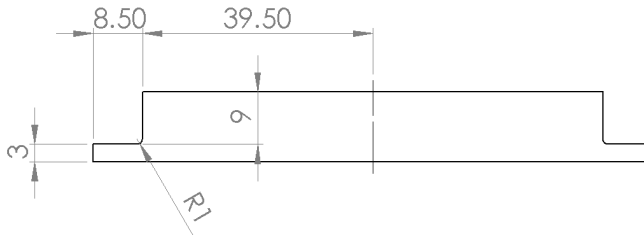


Figure 11: Dimensions for the design space (top view) [mm].

3.1.2 Loads

The most demanding loads that the satellite will experience come from the launch into space. During the launch, the satellite will be mounted to a spacecraft which will be subjected to both static and dynamic loads. The loads will be transferred from the spacecraft to the satellite at the interface between the spacecraft and the satellite's adapter to the spacecraft. Arianespace has provided a user's manual, which describes the stiffness and load requirements for auxiliary payloads for the Vega and Soyuz launchers (see Appendix E). There are also requirements regarding vibrations and shocks, but this is beyond the scope of this thesis.

Stiffness Requirements

Stiffness requirements need to be met in order to prevent natural frequencies to form in the auxiliary payloads, which can affect the dynamic behaviour of the launcher. The minimum requirements are:

$$\begin{aligned} \text{Lateral frequencies:} & \geq \mathbf{45 \text{ Hz}} \\ \text{Longitudinal frequencies:} & \geq \mathbf{90 \text{ Hz}} \end{aligned}$$

Design Loads

The dynamic and static loads from the spacecraft, including the gravity load, can be written as quasi-static loads (QSL), as seen in table 2. The loads are acting on the payload center of gravity (CG) and the lateral loads can act in any direction together with the longitudinal loads. On top of these loads, peaking line loads can be up to 50 % higher than the given design loads. A minimum factor of safety of **1.25** is also required.

Ground and flight load cases	QSL (g) (Static + Dynamic)		
	Longitudinal		Lateral
	Compression	Tension	
Case 1	-14.2	+10.3	+/- 2.6
Case 2	-10.0	+10.0	+/- 4.0

Table 2: Design load cases. Reconstructed from table 4.2.5 in Appendix E.

From figure 12, it can be seen that there are several available mounting positions for the payload on the launchers, and thus there is no guarantee which direction the satellite will be mounted. Since there are no loads specified for the vertical direction, the lateral forces are therefore assumed to act in this direction as well. This gives the possible combination of forces seen in table 3. Here, + indicated tension and - indicates compression.

Using a mass of 6 kg , a gravitational acceleration of 9.81 m/s^2 and a safety factor of 2, the values used can be seen in table 4. In the longitudinal direction, the forces that create tension in the part will be directed in the positive direction, while the compression forces will act in the negative direction.

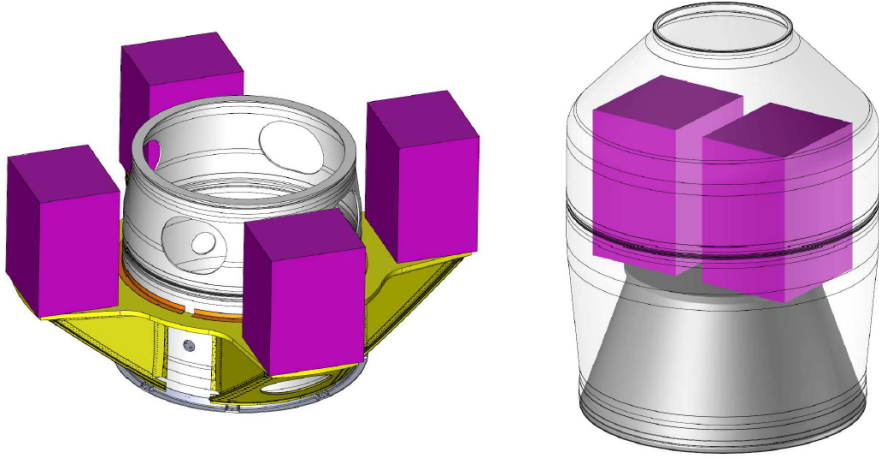


Figure 12: Usable volume for micro auxiliary passengers on the Soyuz and Vega launchers. Gathered from Appendix E.

Case	#	Longitudinal	Lateral	Vertical
1	1	+	+	+
1	2	+	+	-
1	3	+	-	+
1	4	+	-	-
1	5	-	+	+
1	6	-	+	-
1	7	-	-	+
1	8	-	-	-
2	9	+	+	+
2	10	+	+	-
2	11	+	-	+
2	12	+	-	-
2	13	-	+	+
2	14	-	+	-
2	15	-	-	+
2	16	-	-	-

Table 3: Load cases.

Case	#	Longitudinal [N]	Lateral [N]	Vertical [N]
1	1	+1213	+306	+306
1	2	+1213	+306	-306
1	3	+1213	-306	+306
1	4	+1213	-306	-306
1	5	-1672	+306	+306
1	6	-1672	+306	-306
1	7	-1672	-306	+306
1	8	-1672	-306	-306
2	9	+1177	+471	+471
2	10	+1177	+471	-471
2	11	+1177	-471	+471
2	12	+1177	-471	-471
2	13	-1177	+471	+471
2	14	-1177	+471	-471
2	15	-1177	-471	+471
2	16	-1177	-471	-471

Table 4: Calculated values for the load cases.

3.1.3 Materials

The material chosen for this analysis is EOS Aluminum AlSi10Mg. This is an aluminum alloy which is used on some of EOS's DMLS machines. The complete datasheet can be seen in Appendix F.

Because this part is thought to be produced using additive manufacturing, an orthotropic material model will be used. For an orthotropic material, Hooke's law can be rewritten as [18]:

$$\begin{pmatrix} \epsilon_{11} \\ \epsilon_{22} \\ \epsilon_{33} \\ \gamma_{11} \\ \gamma_{22} \\ \gamma_{33} \end{pmatrix} = \begin{bmatrix} \frac{1}{E_1} & -\frac{\nu_{12}}{E_2} & -\frac{\nu_{13}}{E_3} & 0 & 0 & 0 \\ -\frac{\nu_{12}}{E_1} & \frac{1}{E_2} & \frac{\nu_{23}}{E_3} & 0 & 0 & 0 \\ -\frac{\nu_{31}}{E_1} & \frac{\nu_{23}}{E_2} & \frac{1}{E_3} & 0 & 0 & 0 \\ 0 & 0 & 0 & \frac{1}{G_{12}} & 0 & 0 \\ 0 & 0 & 0 & 0 & \frac{1}{G_{13}} & 0 \\ 0 & 0 & 0 & 0 & 0 & \frac{1}{G_{23}} \end{bmatrix} \begin{pmatrix} \sigma_{11} \\ \sigma_{22} \\ \sigma_{33} \\ \sigma_{12} \\ \sigma_{13} \\ \sigma_{23} \end{pmatrix} \quad (16)$$

As such, in order to define an orthotropic material, values for Young's modulus, the shear modulus, and Poisson's ratio are needed in these directions. While E_1, E_2 and E_3 are given, the values for the shear modulus and Poisson's ratio are not. The values for these properties are therefore assumed based on typical values for isotropic aluminum. It should be noted that this assumption could be inaccurate due to the properties of AM. This consideration is therefore limited to heat-treated parts only. The values used can be seen in table 5. The directions 1, 2 and 3 correspond to the longitudinal, lateral and vertical directions respectively.

Property	Value
E_1	70 GPa
E_2	70 GPa
E_3	60 GPa
G_{12}, G_{13}, G_{23}	26 GPa
$\nu_{12}, \nu_{13}, \nu_{23}$	0.33
ρ	2.67 g/cm ³

Table 5: Material properties for AlSi10Mg.

3.1.4 Analysis Setup

The analysis has been set up in Abaqus 2017. The setup can be seen in figure 13, where X, Y and Z represents the longitudinal, lateral and vertical directions

respectively. Only one side of the satellite has been modelled because of symmetry over the mid-plane of the satellite. Bolts have also been added to capture the effects of the loads and boundary conditions being transferred to the design space from the attached components. The outer countersunk bolts represent the connection to the system outside the payload assembly, and is assumed to be rigid. The threads of these bolts are therefore fully fixed. To model that the loads are acting on the payload center of gravity, a reference point at this location has been added. This point is connected to reference points at the end of the inner bolts via connectors. These connectors will transfer axial loads, as well as any rotation experienced by the CG. The connector type used is "link" for the translation and "rotation" for the rotation. The end of the bolts are coupled to the threads by a continuum coupling. Each load case is defined as a linear perturbation step so that they are calculated independently of each other. Pretension in the bolts were not added in this analysis. This is because the nodes around the bolts would have been part of both a pretension load and from a connector, and this was not allowed by Abaqus. The bolt loads were therefore excluded. The complete setup can be seen in Appendix A. For previous models used, see Appendix C.

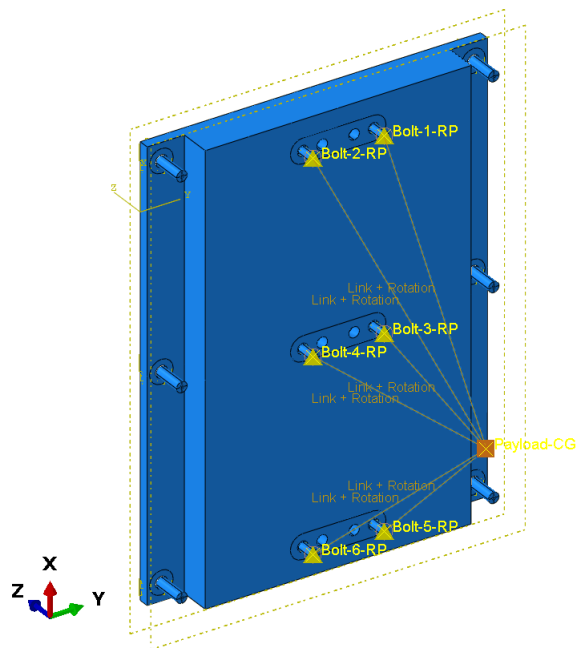


Figure 13: Interactions in Abaqus, seen from the backside of the design space. X - longitudinal, Y - lateral, Z - vertical.

3.1.5 Optimization Setup

The objective of this optimization process is to maximize the stiffness of the components. In other words, a typical minimum compliance problem. This is equivalent to minimizing the strain energy. As such, this becomes the objective function for the problem. In order to preserve the geometry in certain areas, these areas are considered to be "frozen", which mean that they can not be modified during the optimization process. The only constraint applied to the problem is a weight constraint of maximum 36 grams. This optimization used a sensitivity-based algorithm with SIMP as the material interpolation technique. A penalization factor of 3 was used. Because the load cases are linear perturbation steps, each load case is optimized separately. Default convergence criteria were used. After the optimization process is complete, the results from each load case are combined into one final result. Appendix A.8 covers the settings used in the optimization process in more detail. The optimization was set up in Abaqus, and then Tosca Structure was used for the calculations in the optimization process.

3.1.6 Frequency Analysis

The natural frequencies were calculated in Abaqus for each of the finished components after post-processing. A linear perturbation frequency step was used. In the setup, no loads were used. For the boundary conditions, the bolts were removed and only the surface that would have been in contact with the heads of the countersunk bolts were fixed. See figure 14. The bolts were removed so that no other component would influence the frequencies of the part. The first five eigenfrequencies of the all the parts were found.

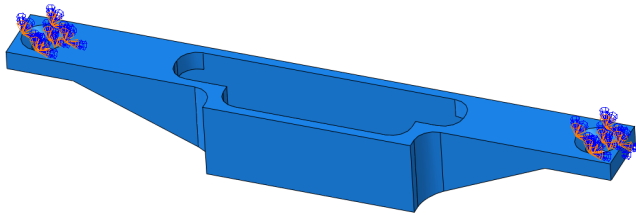


Figure 14: Boundary condition during the frequency analysis.

3.2 Post-processing

After a final optimization result is obtained, the model must be post-processed. While a full CAD regeneration will often yield the best results, it is very time-consuming. This post-processing process has therefore been focused on using a more simple approach by utilizing the reverse-engineering capabilities of modern CAD programs. The following approach was used:

1. Extract the results as an STL file from Tosca using smoothing and filtering cycles.
2. Further smooth local areas and use symmetry planes to cut the model in Autodesk Fusion 360.
3. Convert the STL file to an OBJ file made up of quadrilaterals in Autodesk ReCap Photo.
4. Convert the mesh body into an editable T-spline body in Fusion 360. Make adjustments by moving, rotating and scaling vertices, edges and faces.
5. Convert the T-spline body into a solid body by boundary representation (BRep).
6. Regenerate areas of importance, such as bolt holes, by solid modeling in any CAD program of choice. Mirror the body using the symmetry planes used earlier to reestablish a complete model.

Tosca Structure has built-in tools to extract the optimization results into an STL file. By using this extraction tool, parameters such as iso-value, the number of smoothing cycles, filtering, and which design cycle the results are extracted from can be adjusted. The iso-value is used to calculate the position of new nodes on the interior edges of elements [19]. The default iso-value is 0.3. Increasing this value will shift the surface toward the inside of the model while decreasing it will shift it outwards. Changing the iso-value will therefore change the model volume. Figure 15 shows the effect the number of smoothing cycles has on the model. A higher number of smoothing cycles will give a smoother surface, but it can also cause thin members to contract. Smoothing should thus be used with caution. Filtering can be used to remove flaws or irregularities in the model. 5 smoothing cycles, as well as moderate filtering and an iso-value of 0.3, was used for the final extraction.

After surface extraction from Tosca, the model is still in need of further editing. The smoothing cycles from the extraction did not give the desired result all over the model, and so further smoothing has been used to clean up undesired sharp edges due to the triangular representation of the STL file. Autodesk's Fusion 360 was used for this process, but there is a number of different software that can be used to edit mesh bodies, like MeshLab and Meshmixer. During this step, the

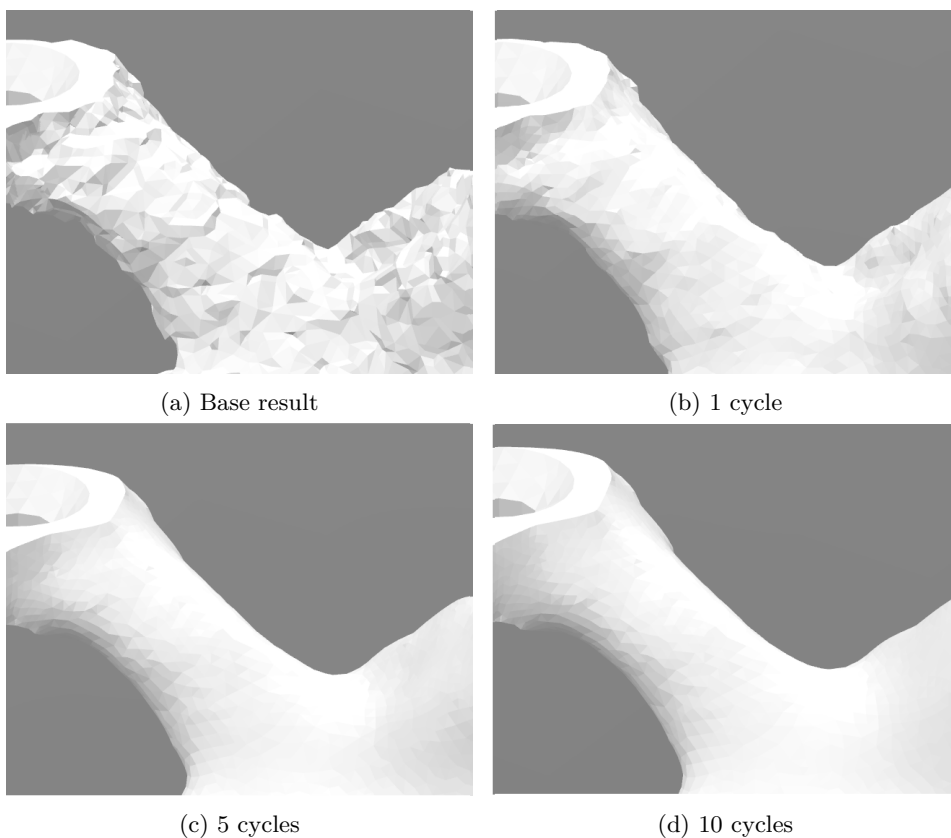


Figure 15: The effect of smoothing cycles.

model was also cut using symmetry planes. This will speed up the post-processing process and will cause the final result to become fully symmetric over the planes used. This will, however, cause deviation from the optimization results. At this point, the model is still saved as an STL file.

Fusion 360 has features within its sculpting environment to edit certain bodies. To access these features, however, the body must be a so-called T-spline body. Mesh bodies can be converted to T-splines, but only mesh-bodies from quad-based OBJ files. As such, the STL file is converted to an OBJ file using Autodesk's ReCap Photo. This file is then brought back into Fusion and converted to T-splines. This body is made up of a grid of control points. These points, along with the edges and faces, can be edited by translation, rotation and scaling operations. Due to the high number of these control points, each edit operation is slow which makes this step very tedious.

After the final adjustments have been made to the general shape of the model, it

can be converted to a solid body, or a BRep body as it is known in Fusion. This model can be saved as a STEP file, which can be imported into any CAD program. Final modifications to the model using standard solid modeling features can then be made in areas of interest. In this case, NX was used to regenerate all bolt holes, as well as the areas around the holes. Finally, the solid body was mirrored across the symmetry planes to create a full body.

The final post-processed parts can be seen in figures 16 - 18. Figure 19 shows a comparison of the one-piece bracket before and after post-processing. Due to the symmetry, the top and bottom brackets are identical. Further details about the post-processing steps can be found in Appendix B.



Figure 16: Render of the finished one-piece bracket.



Figure 17: Render of the finished center bracket.

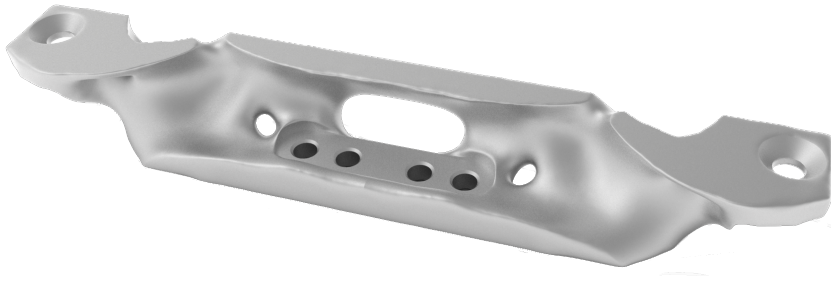
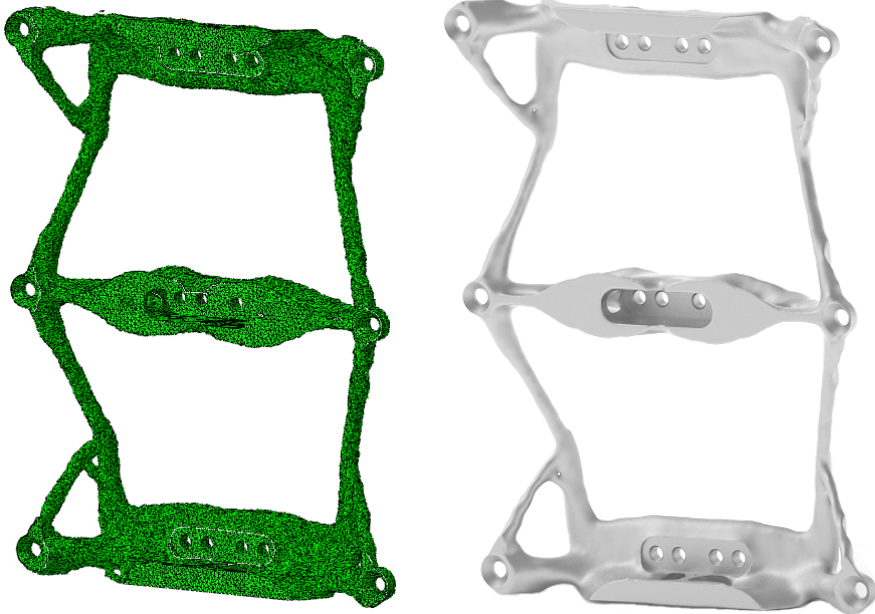


Figure 18: Render of the finished top and bottom brackets.



(a) Before post-processing

(b) After post-processing

Figure 19: Before and after post-processing of the one-piece bracket.

4 Results

4.1 Optimization Results

The optimization results from Abaqus/Tosca can be seen in figure 20 and 21 for the one-piece and the individual brackets respectively. Plots for the strain energy and weight during the optimization process can be seen in figure 22 and 23. The main difference between these results is naturally the members connecting the upper and lower parts to the center. Aside from this, the two results show many of the same trends in the mutual areas. As expected, the individual brackets are bulkier as the same amount of material is distributed over a smaller volume. Both results are close to symmetric, but not completely. This is because the loads in the longitudinal direction are not symmetric. The process can also have converged on a local solution, and not a global one in those areas.

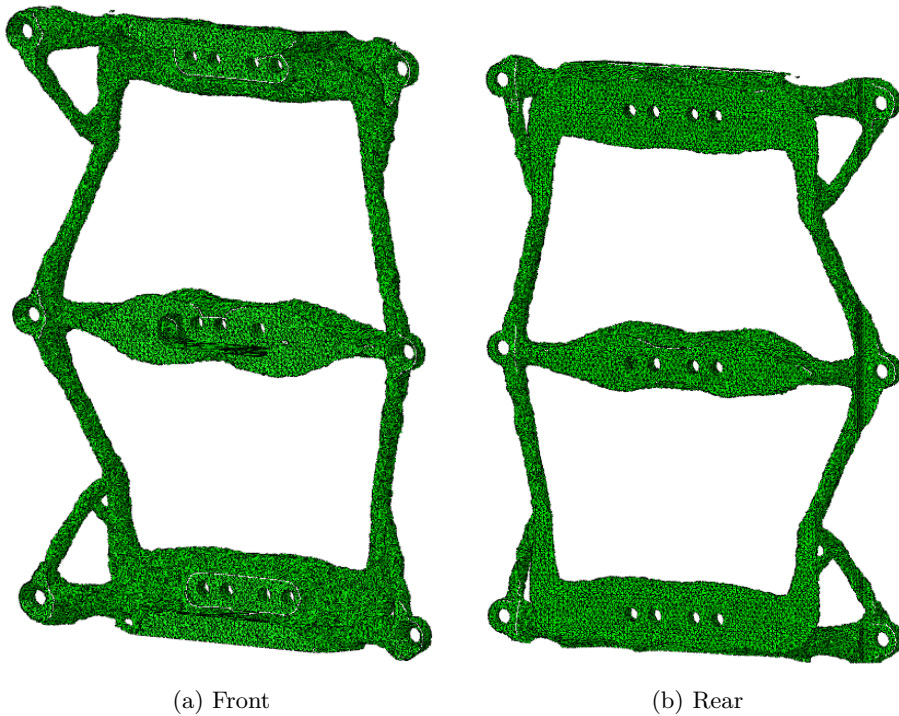


Figure 20: Optimization results of the one-piece bracket.

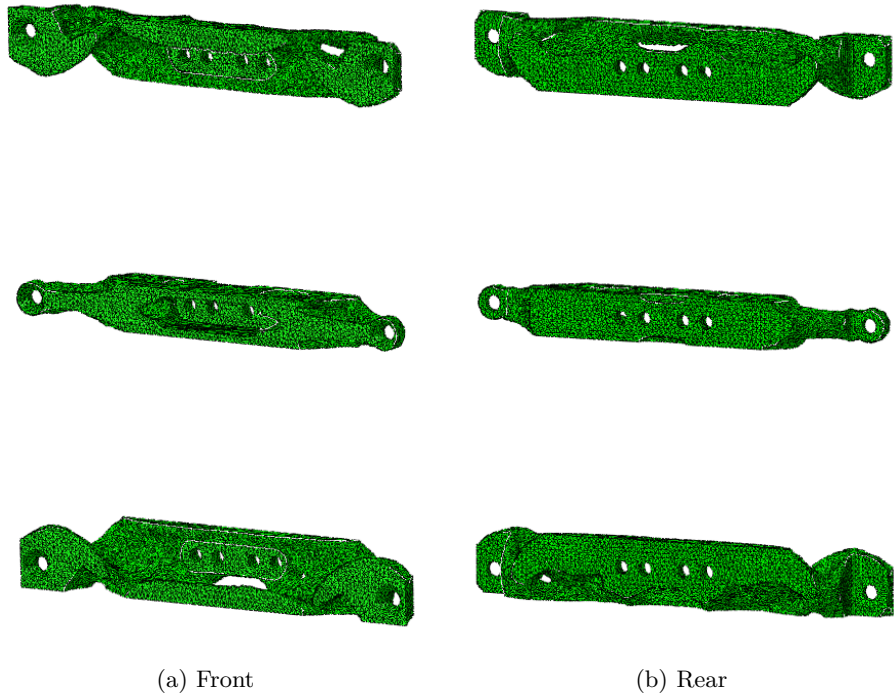


Figure 21: Optimization results of the individual brackets.

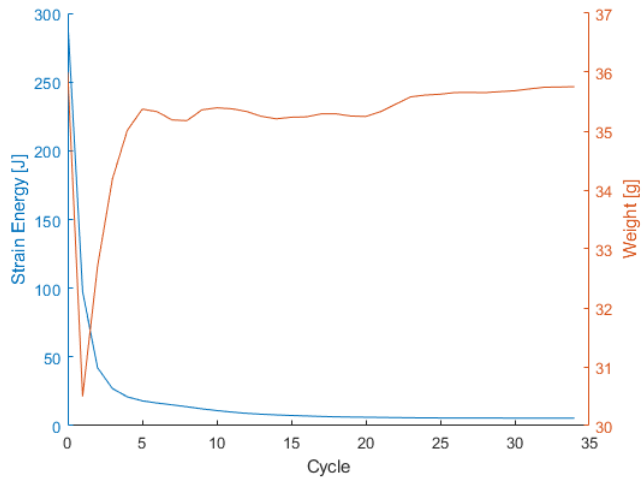


Figure 22: Plot of the weight and strain energy during the optimization process for the one-piece bracket.

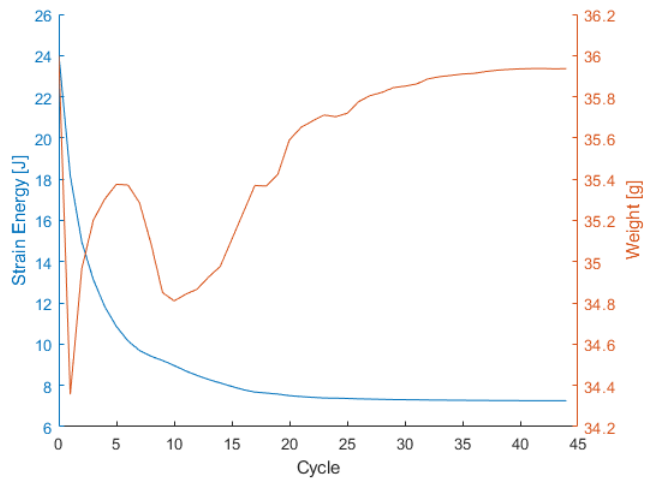


Figure 23: Plot of the weight and strain energy during the optimization process for the individual brackets.

4.2 Stresses and Strains

As part of the optimization process, the stresses and strains are calculated for each design cycle. The stresses for the final results after the load cases have been combined can be seen in figure 24. The strains can be seen in figure 25. The one-piece bracket experiences both lower peak stresses and strains than the individual brackets. As expected, these stresses occur around the bolts. The general stress level in the components are however more similar, and the stresses follow the same trends. While the same is true for the strain trends, both the general level and peak strains in the individual brackets are higher.

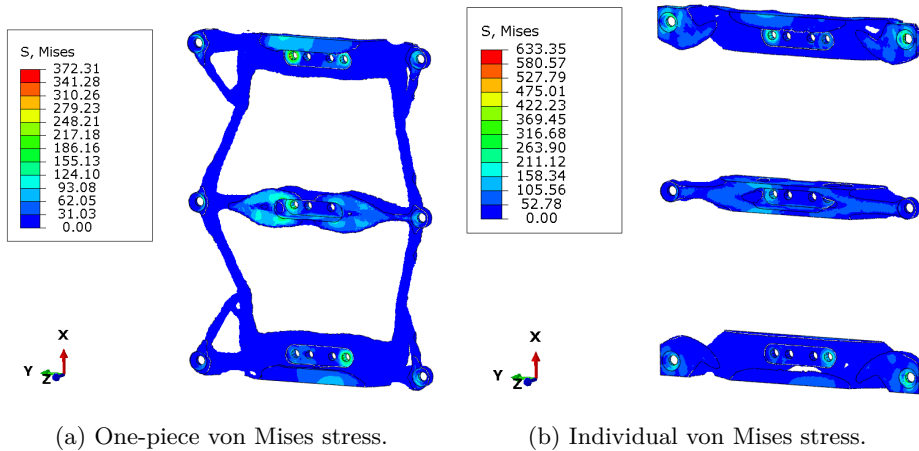


Figure 24: Von Mises stresses [MPa] after combination.

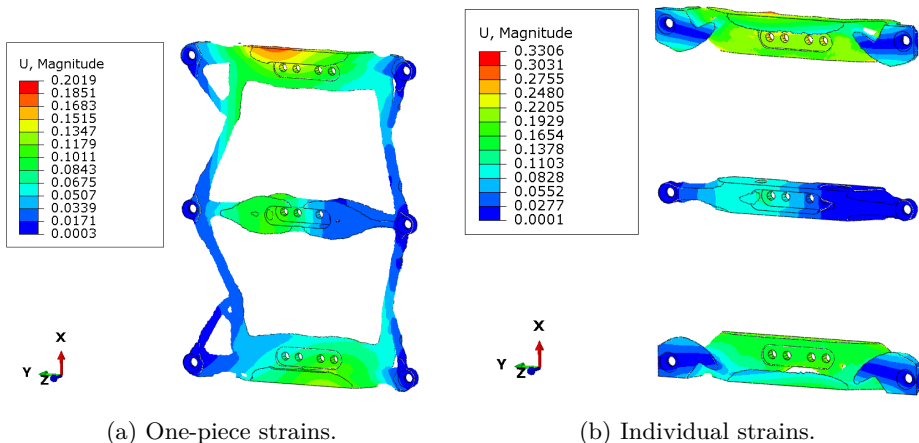


Figure 25: Strains after combination.

Due to the excessive safety factors used, these values cannot be used as a failure criterion. A weight of 6 kg with an additional safety factor of 2 was used for the load as described in section 3.1.2. However, this is the weight of the entire satellite. The weight of the payload is ca. 520 g, which means that a safety factor of 23 has been used in reality. For real verification purposes, a much lower safety factor should be used, and all the load cases should be evaluated separately. Because an orthotropic material model has been used, the Tsai-Wu failure criterion should also be considered over the von Mises criterion.

4.3 Natural Frequencies

While the natural frequencies are a design requirement, it can also be a useful measurement of the stiffness of the components. The results for the optimized components compared to their respective base components can be seen in tables 6-8. The final weight of each component is also listed. While all the optimized components have a higher natural frequency in the first mode than their original counterparts, the original brackets have higher frequencies in the higher modes. The new center and top/bottom brackets have higher frequencies in mode 1 and 2, while the one-piece bracket only has a higher frequency in the first mode when compared to all the original brackets. All the optimized components have a higher weight than the original parts. The combined weight of the optimized separated brackets is 43.4 g, while the three original brackets add up to 35.7 g. All the components satisfy the stiffness requirements from section 3.1.2.

Mode	Original Center	New Center
1	3224.4 Hz	3849.3 Hz
2	5164.9 Hz	5422.5 Hz
3	7176.5 Hz	6204.2 Hz
4	10654 Hz	9579.9 Hz
5	12053 Hz	10949 Hz
Weight	10.7 g	11.6 g

Table 6: Comparison of the natural frequencies and weight between the original and new center bracket.

Mode	Original Top/Bottom	New Top/Bottom
1	2667.4 Hz	4137.5 Hz
2	4821.1 Hz	6387.7 Hz
3	7595.8 Hz	6921.4 Hz
4	9162.9 Hz	7739.9 Hz
5	11325 Hz	11423 Hz
Weight	12.5 g	15.9 g

Table 7: Comparison of the natural frequencies and weight between the original and new top and bottom brackets.

Mode	One Piece
1	3795.4 Hz
2	4172.6 Hz
3	4186.2 Hz
4	5016.6 Hz
5	5032.5 Hz
Weight	39.9 g

Table 8: The natural frequencies and weight of the one-piece bracket.

4.4 Manufacturing

When using additive manufacturing to produce parts, an important aspect is the part orientation during manufacturing. This is important both in terms of the anisotropic properties, but also with regards to support material. Due to the several overhangs in the parts, support material will be needed if a DMLS process is used. Figure 26 shows the result after an orientation analysis on the one-piece bracket done in Autodesk Netfabb with a critical support angle of 45° . Figure 26a shows the optimal orientation for the least amount of support volume, while figure 26b shows the best result for the least amount of support area on the part. Other intermediate results are also available. Figure 27 shows where the support areas for the two orientations would be. In table 9, the required support area, support volume, outbox volume and part height for the two orientations can be seen. The outbox volume is the volume of a virtual box that encompasses the part. In other words, it is the total volume the part needs in a machine.

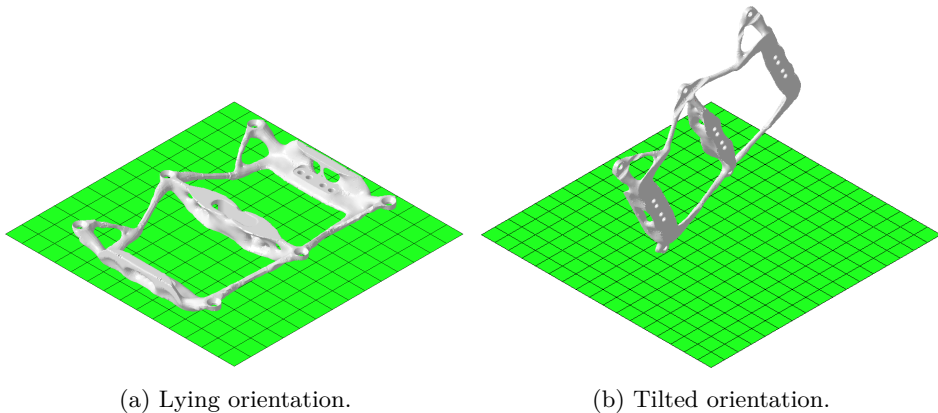


Figure 26: Different optimized print orientations.

After manufacturing, the supported areas will often leave a higher surface roughness than the other surfaces on the part. This is not desirable both in terms of the appearance and the fatigue strength. However, choosing the orientation with a lower support area greatly increases the support volume, outbox volume, and part height. This will lead to a higher production time and also reduce the number of parts that can be manufactured at the same time. The orientation of the material model was based on the lying orientation.

Orientation	Support Area	Support Volume	Outbox Volume	Part Height
Lying	36.446 cm^2	7.909 cm^3	142.084 cm^3	12.1 mm
Tilted	8.511 cm^2	29.011 cm^3	349.39 cm^3	137.1 mm

Table 9: Support info for the two orientations.



(a) Lying orientation.

(b) Tilted orientation.

Figure 27: Support areas for the different orientations marked in red.

5 Discussion

5.1 Problem Setup

One of the most critical aspects when setting up a topology optimization is the design space. Although the optimization process may find an optimal solution for a given design space, a better solution to the problem can still exist. Because of this, a restricted design space can restrict the performance of the final result. In this case, the design space was determined by the limits of the original brackets. Some small adjustments were made, as described in section 3.1.1. As seen from the results, the final geometry is pushed up to the surfaces of the design space on both the front and back and also to some degree on the filleted edges. This is an indication that the design space may be too small. If the design space had been extended further in these directions, the solution would probably have added more material there. A good example of this is seen in figure 28. Here, the design space was extended by the distance L . Instead of cutting off the material at line B, the solution stopped more "naturally" before line A. In the case of the brackets, the backside will always be present since this is a contact surface with other components. The front surface could potentially have been moved. However, this work has been done without the knowledge of the surrounding components, so this was not done. In an actual product development scenario, this would probably have been different and the design space could have been adjusted.

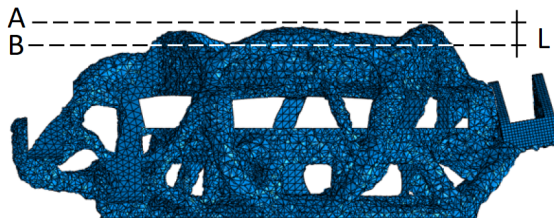


Figure 28: The effect of an extended design space from A to B. Used with permission from Thomas Herstad.

Another element to consider when choosing the design space is the ratio between the target volume and the available volume in the design space. If this ratio is too low, the results will result in very thin members. This can be a limiting factor for the stiffness and natural frequency of the component, as described in section 2.2. This may be one of the reasons why the natural frequency of the top and bottom brackets is higher than the natural frequencies than the one-piece bracket.

For this problem, an orthotropic material model was used based on the material data from Appendix F. As described in 3.1.3, only Young's modulus is given in the X, Y and Z direction, while the values for the shear modulus and Poisson's

ratio are assumed based on typical values for isotropic aluminum. This assumption was made mainly because it seems that it is very difficult to find these values from scholarly sources for additive manufactured aluminum. It is also hard to find these values for steel and titanium alloys, even if these materials seem to be of a higher academic interest. Most of the articles on the mechanical properties of additive manufactured materials seem to focus on yield and ultimate strength, Young's modulus, elongation, and hardness. An article on the mechanical properties of selective laser-melted (SLM) steel reported values for Poisson's ratio between 0.170 and 0.444 [20], compared to a typical value of ca. 0.3. This indicates that the assumption of a constant Poisson's ratio may not be very good. After the final results were obtained, however, one source on AlSi10Mg was discovered. Here it was reported that Poisson's ratio for the material varied between 0.2901 and 0.3619 with SLM, depending on the direction [21]. Although there is a fluctuation in the values, the deviation from 0.33 that was used in the optimization is much smaller than the deviation for stainless steel. The case for the assumption is now stronger, but it is now obvious that these values should have been used for the optimization processes. Regardless, it is difficult to predict the effect these values would have had on the final result. Ideally, a new optimization should have been done. The results could then have been compared to the current results. The results could also have been compare to the results from an optimization for an isotropic material model to see if it makes any difference with an orthotropic material model.

A major challenge with topology optimization is to find and model all the possible load cases for the selected component. Because the optimization algorithm only leaves material where it is necessary, loads that stress the component in a different way than it was optimized for can be catastrophic. If some load cases are left out of the optimization or modeled incorrectly, the component may fail once these loads are applied. Although this is also true for components designed using traditional design methods, these components tend to have a higher safety factor to other loads due to the generally less optimal design. Because of this, all the 16 load cases for this problem were included in the optimization. Another approach could have been to find the most critical loads and then only use these. While this could have given good results, the component would in all likelihood be weaker against some of the load cases that would have been left out. Alternatively, all load cases could have been included, but with different weighting depending on the severity of the load cases. This would have ensured that the component would still perform well with the most critical loads, while it could also handle the other loads. The challenge with this approach would be how each load case is weighted. The more load cases there are, the more challenging this would be. The weighting of the lower weighted load cases could potentially be very close to zero if the sum of all load cases equals 1. The weighting would have to include both the severity of the load cases in terms of factors such as stress, but also the frequency of which the load appears. A load that is present for much of the lifetime of the component should be considered important. A load that causes high stresses, but would seldom appear should also be of high importance. Although weighting the load cases would be challenging, it could still be a better approach than the linear weighting that has been used for

this problem.

As mentioned in section 4.2, the safety factor used for the optimization is around 23, which is excessively high. One of the reasons why this was used was to "force" the optimization to produce a result with a higher stiffness. If the actual weight of the payload (520 g) had been used, the largest force would have been ca. 145 N with a safety factor of 2. Because the optimization algorithm will create a structure that can handle the loads, very low loads can lead to thin structural members. As described in section 2.2, thin members will lead to a lower natural frequency. By using higher loads, thicker members will form, and the natural frequency will increase. An alternative method could have been to use a lower safety factor and implement a minimum member size constraint in the optimization. Figure 8 in section 2.2 could have been used to determine the minimum member size to use for this constraint if the lowest desired natural frequency, as well as an approximate maximum member length is known. The latter can, however, be difficult to predict. A minimum member size could also be useful in order to get a result that has better manufacturability.

With regards to natural frequencies, another approach for the optimization could be to use eigenfrequency, called "Eigenfrequency calculated with Kreisselmeier-Steinhauser formula" in Abaqus (see figure A.29), as a design response and set up the objective function to maximize this response. By using this approach, the lowest natural frequency will be maximized. During the optimization, the modes will be weighted according to their distance to the lowest frequency. The modes may also switch places during the optimization. E.g. the first mode can be maximized, leaving the second mode as the mode with the lowest frequency. It could be interesting to investigate the difference between the results of a maximum frequency and a minimum compliance optimization. However, previous attempts with the maximum frequency optimization have not produced good results.

In section 3.1.1 it was mentioned how the design space was made symmetric. However, no symmetry planes were used to cut the design space. Even though the part is symmetric, the loading is not. If a quarter of the design space had been used, symmetry boundary conditions would have been used on both the symmetry planes of the design space, but also on the payload CG in order to prevent rigid body motion and subsequent numerical singularities. If the CG had been constrained from movement in two directions, the forces applied would not yield any results as the strain from the CG would be zero. Thus, this would have caused parts of the load cases to effectively be excluded from the optimization.

5.2 Results

Topology optimization results are usually very organic and unintuitive, which makes them hard to analyze with engineering judgment. A potential problem with the optimization is that the algorithm can end up converging on a local solution, rather than finding the global optimum for the problem. If the constraints used are too strict, the global solution can end up outside the given constraints and thus a local solution will always be found. In this optimization, the only constraints are the weight target and the frozen areas in the design space. When comparing the results, the top and bottom parts are very similar which is an indication that more or less the same solution has been found for both problems. When looking at the center part of the one-piece bracket in figure 29, it is clear that the solution on the left and right sides are different, even if both the design space and the load cases are symmetric across the center plane. This can be a suggestion that local solutions were found on each of the two sides. The bottom left quarter from this figure was used for the post-processing.

Another issue to have in mind when working with topology optimization is the mesh dependency of the results. While it is possible to get good results in FEA with a coarse mesh, this is often not the case for topology optimization. Because elements are added or subtracted during the optimization process, the size of the elements will have a great impact on the final structure. The same trends can often be seen with different element sizes, but the formation of holes or thinner members may only be seen with a fine mesh. It is obvious that members or holes smaller than the element size cannot be formed. For this project, elements of 1 mm were used for the design space. The results from this mesh and another one with an element size of 2 mm were very similar. It could therefore be postulated that a certain critical element size exists for each problem. A finer mesh will, however, increase the computational time and cost of the optimization.

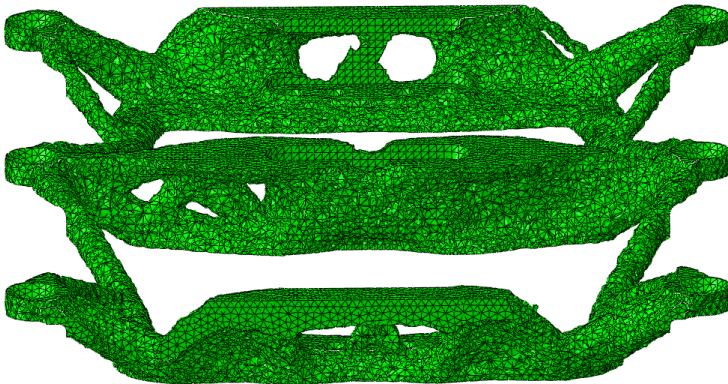


Figure 29: Tilted view of the one-piece bracket in Abaqus.

To verify the result, FEA should be used. The results in section 4.2 show very high peak stresses in the parts. However, given the high safety factor that was used, it gives confidence that the parts will be in no danger of failing during the real load cases. In order to fully verify the strength of the components, a new analysis of all the load cases with an appropriate safety factor should be considered. Nevertheless, the static results available show that the general stress levels in the parts are very low. The peak stresses are locally around the bolt holes, as expected. With pretension in the bolts, the stresses would have been even higher around the bolts. Because there is already a lot of material in these areas, the optimization would probably not have added much more there.

Although the stresses are assumed to be very small with the real forces, an issue that could be taken into account is fatigue. From Appendix F, it is reported that the fatigue strength of AlSi10Mg after 5 million cycles was 97 ± 7 MPa in the as-built condition. The total time the satellite is affected by the launch loads is not very long, but the frequency of the loads is likely very high. To do a full fatigue analysis, these factors should be known. Because the fatigue strength is reported for the as-built condition, physical testing of the components after heat treatment would be the best way to ensure no fatigue failure will occur during launch.

A surprising result is in the natural frequencies of the parts. As expected, all the optimized results achieved higher frequencies than the original parts. It was initially expected that the one-piece part would have the highest frequencies of the optimized parts. In fact, the results show that this was the part with the lowest natural frequency of all the optimized parts. The assumption was that with the parts connected, the one-piece bracket would achieve a higher stiffness than the separated brackets. The lower frequencies are likely a product of the thinner members on this part compared to the other bulkier parts.

Another interesting observation is that even though the one-piece bracket has a lower natural frequency than the separated brackets, the peak strain is lower. The strain trends seem to be the same for both results, but the general level is also higher in the separated brackets.

One point to remark is the increased weight of the optimized results. From figure 22 and 23, it can be seen that both optimization processes were completed with a weight lower than the target of 36 g. After post-processing, however, the weight increased. While more material could increase the stiffness of the part, the mass in itself will cause a decrease in the natural frequency as seen from equation 11 in section 2.2. The net effect of the increased weight is therefore hard to determine.

In the optimization, no manufacturing constraints were used as the results were intended to manufacture using AM. Although the costs to produce parts with AM is generally higher than using traditional manufacturing methods, the difference is smaller if the number of components is smaller, as mentioned in section 1.4.4. If these parts were to be produced, only two sets of parts would be needed. If

the performance of the parts is higher than what could be achieved without AM, then this could help to justify the price difference. However, with AM the material properties would be unpredictable and inferior to in many cases. After the AM process, it would be preferable to do post-machining. The areas around the bolts and the contact surfaces would clearly benefit a few passes with a milling machine, even though this would further increase the cost. The machining would, however, increase the fatigue strength as mentioned in section 1.4.1.

5.3 Post-Processing

The biggest challenge with the post-processing step is reconstructing the geometry as highly organic shapes are generally difficult to model with CAD software tools. It was initially attempted to use the reverse engineering tools in NX to model the components. In NX it is possible to create splines directly on the mesh body which can then be used for operations such as lofting, sweeping or extrusion. For some reason, possibly because of errors in the STL file, this would only work on parts of the model. This approach was subsequently aborted. Another approach by using the sculpting tools in Fusion 360 was also attempted. However, when working with mesh bodies in Fusion, design history cannot be captured. This makes it very time consuming to edit the model to fix previous mistakes, especially with little experience with the sculpt tools. Other programs like 3DEXPERIENCE CATIA are apparently well suited for CAD regeneration, but this was unavailable during this process. Paramatters is another software that is claimed to produce topology optimized parts that are ready for manufacturing without the need for manual post-processing [22].

Due to the approaching deadline, a quicker and more automatic approach to the reconstruction was used, as described in section 3.2. While the results were good, there were some issues with this method. The first issue was that the solid body conversion and the saved STEP file was not perfect. When opening the final STEP file in SolidWorks, one of the models contained some self-intersecting faces and some missing faces. This could fortunately be fixed automatically by using the import diagnostics in SolidWorks. The second problem was discovered when the parts were imported into Abaqus for the final frequency analysis. Because the solid model was converted using boundary representations of the geometry, some of the feature edges and faces created are not well defined. This led to problems with the subsequent meshing of the parts, as seen in figure 30. This mesh used the same settings as in the initial optimization (see figure A.27), but the quality of the mesh is much worse. This is something that could have had an impact on the final results. The final issue from this method is the file sizes. The STEP files are 75 MB, 58 MB and 50 MB for the one-piece, top/bottom and center brackets respectively. Although it is difficult to estimate the size of the parts if they had been created using traditional solid or surface modeling, these file sizes are very large compared to "normal" parts. This is likely because the geometry is based on

the triangular representation of the STL files instead of parametric functions.

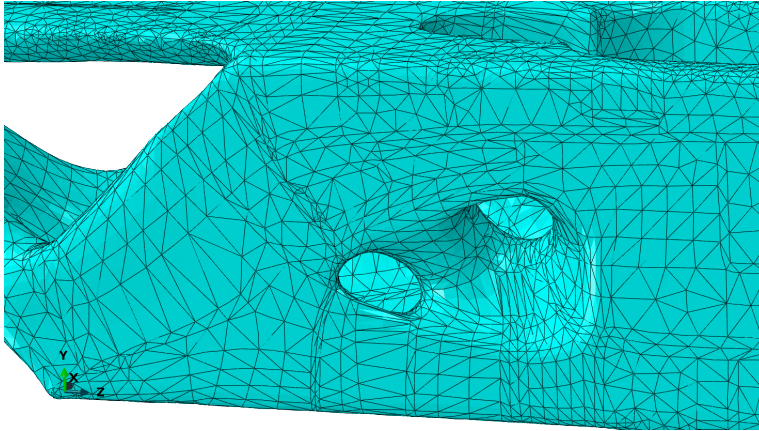


Figure 30: Mesh on the new center bracket.

The added mass of the finished parts has been traced back to the original mesh body extracted from Tosca. The base result without any smoothing or filtering with a default iso-value of 0.3 was measured to 44.33 *g* in SolidWorks. This is the result which is presented in Abaqus by default (figure 20 and 21). It is clear that the weight calculated for the constraint in the optimization is different from the weight of the mesh body presented in the results. Although this extra weight is only 8.33 *g*, it still amasses to over 23 % above the target. To counteract this problem, either a higher iso-value can be used when extracting the results, or a lower target weight can be used.

A general problem with the post-processing step is that as soon as the model is changed, there will be a deviation from the "optimal" solution from the topology optimization process. There will always be some elements of the solution that has to be changed due to the mesh based result, like circular holes. Other changes will be done either to make it more suited for manufacturing or to make it more pleasing to the eye of the constructor. It may take some time before a fully automatic CAD regeneration is possible, but in this work, it has been shown that post-processing is possible without having to manually reconstruct all the features of the geometry. The results are obviously not perfect, but in terms of time and effort saved it still serves as a good solution. As both topology optimization and 3D scanning become more popular, the reverse engineering tools in the CAD packages will become better and more easy to use.

A proposed alternative post-processing approach is to use software dedicated to digital sculpting and modeling instead of traditional CAD software for highly organic shapes. Software like Modo and Autodesk Maya are some examples. These programs are made for artists to create models for movies, games, and animations, and are specialized to create organic models. Thus, the sculpting and organic

modeling tools in these software packages are far beyond the capabilities found in modern CAD software. After the general shape is reconstructed with this approach, features such as holes, slots, and threads could be added to complete the model.

6 Conclusion

With the use of topology optimization in Abaqus and Tosca Structure, two different optimized solutions have been made and compared to three previously engineered mounting brackets for the payload in the AISSat 1 satellite. By using a minimum compliance problem and a sensitivity-based algorithm, the stiffness of the optimized components surpassed the original parts. The natural frequency of the components was used to compare the results. While the frequency of the first mode of the eigenvalues of the optimized components was higher, the original brackets had higher frequencies for modes 3-5. Because the components are not highly stressed, the optimized results and the original parts were only compared in terms of natural frequencies. The optimized components did not meet the weight target due to inconsistencies in terms of mass calculation of the results in the optimization software. The results were post-processed without using a full manual reconstruction of the geometry.

After comparing the two different results, the individual brackets seem to be the best choice for if these parts would have been produced for actual use. These brackets have higher natural frequencies, but would add 4.4 gram compared to the other solution. In addition to the increased stiffness of these brackets, there is another advantage with these parts. The thicker members will increase chances that the parts will be manufactured without errors. Because each part is smaller, there is a possibility that they could also be manufactured together with other parts in the same machine.

The design process when using topology optimization is heavily oriented around a good analysis model where the loads and interactions with other components are accurately modeled. The definition of the design space and the constraints in the optimization model is also crucial in order to achieve good results.

6.1 Future Work

Even though the final results could have been manufactured and used in a real-life setting, there are some final aspects that could be investigated further in order to reduce the risk of failure. This includes a final validation of the stresses for all the load cases and a fatigue analysis. An analysis of the thermal loads could also be considered.

A new optimization process could be started with the correct values for the Poisson's ratio and compared with the current solution. The actual shear modulus should ideally be used, but these values seem to be very difficult to find in scholarly sources. The new optimization should either use a lower weight target or a higher iso-value for the result extraction in order to meet the real weight target.

Other interesting aspects that could be explored is to find the lowest weight of the parts while still achieving the same stiffness and to use manufacturing constraints to find a solution that could be manufactured without additive manufacturing. To find the lowest weight, an iterative approach with several different weight targets would have to be used and then compare the natural frequencies of those results.

References

- [1] *AISSat-1 and 2*. URL: <https://directory.eoportal.org/web/eoportal/satellite-missions/a/aissat-1-2>. (accessed: 01.05.2018).
- [2] *AISSat-1*. URL: <https://en.wikipedia.org/wiki/AISSat-1>. (accessed: 01.05.2018).
- [3] *AISSat-1 tusen dager i rommet*. URL: <https://www.romsenter.no/no/Aktuelt/Siste-nytt/AISSat-1-tusen-dager-i-rommet>. (accessed: 02.05.2018).
- [4] Martin P Bendsøe and Ole Sigmund. “Topology optimization by distribution of isotropic material”. In: *Topology Optimization*. Springer, 2004, pp. 1–69.
- [5] SD Rajan. “Sizing, shape, and topology design optimization of trusses using genetic algorithm”. In: *Journal of Structural Engineering* 121.10 (1995), pp. 1480–1487.
- [6] Haley J McKee and John G Porter. “Lessons Learned in Part Design from Topology Optimization through Qualification”. In: *Science in the Age of Experience* (2017).
- [7] Brett P Conner et al. “Making sense of 3-D printing: Creating a map of additive manufacturing products and services”. In: *Additive Manufacturing* 1 (2014), pp. 64–76.
- [8] NN Kumbhar and AV Mulay. “Post processing methods used to improve surface finish of products which are manufactured by additive manufacturing technologies: a review”. In: *Journal of The Institution of Engineers (India): Series C* (2016), pp. 1–7.
- [9] John J Lewandowski and Mohsen Seifi. “Metal additive manufacturing: a review of mechanical properties”. In: *Annual Review of Materials Research* 46 (2016), pp. 151–186.
- [10] T DebRoy et al. “Additive manufacturing of metallic components—process, structure and properties”. In: *Progress in Materials Science* (2017).
- [11] Jonathan D Hiller and Hod Lipson. “STL 2.0: a proposal for a universal multi-material Additive Manufacturing File format”. In: *Proceedings of the Solid Freeform Fabrication Symposium*. 1. Citeseer. 2009, pp. 266–278.
- [12] D Ma, F Lin, and CK Chua. “Rapid prototyping applications in medicine. Part 2: STL file generation and case studies”. In: *The International Journal of Advanced Manufacturing Technology* 18.2 (2001), pp. 118–127.
- [13] SH Sun, HW Chiang, and MI Lee. “Adaptive direct slicing of a commercial CAD model for use in rapid prototyping”. In: *The International Journal of Advanced Manufacturing Technology* 34.7-8 (2007), pp. 689–701.
- [14] Amit Bandyopadhyay and Susmita Bose. *Additive Manufacturing*. CRC Press, 2016, pp. 277–293.

- [15] Ole Sigmund. “A 99 line topology optimization code written in Matlab”. In: *Structural and multidisciplinary optimization* 21.2 (2001), pp. 120–127.
- [16] Joseph Edward. Shigley, Charles R. Mischke, and Thomas H. Brown. *Standard handbook of machine design*. McGraw-Hill, 2004, p. 133.
- [17] Härkegård Gunnar. *Dimensjonering av maskindeler*. Tapir, 2004, pp. 50–52.
- [18] Arthur Peter Boresi, Richard Joseph Schmidt, and Omar Marion Sidebottom. *Advanced mechanics of materials*. Vol. 6. Wiley New York, 1993.
- [19] *Abaqus 2016 Documentation*. URL: <http://abaqus.software.polimi.it/v2016/index.html>. (accessed: 10.05.2018).
- [20] Leonhard Hitzler et al. “On the anisotropic mechanical properties of selective laser-melted stainless steel”. In: *Materials* 10.10 (2017), p. 1136.
- [21] Leonhard Hitzler et al. “Direction and location dependency of selective laser melted AlSi10Mg specimens”. In: *Journal of Materials Processing Technology* 243 (2017), pp. 48–61.
- [22] *Paramatters, Making Ideas Matter*. URL: <https://paramatters.com/superior-topology/>. (accessed: 10.06.2018).

A Abaqus Setup

This appendix covers the settings used in the setup in Abaqus. The setup consists of the following steps:

1. Part
2. Properties
3. Assembly
4. Step
5. Interaction
6. Load
7. Mesh
8. Optimization

Two Abaqus models were created, one for the one-piece bracket and one for the separated brackets. The settings and setup for these two models are exactly the same. The only difference is the parts used for the design space.

A.1 Part

All the parts were modeled in SolidWorks and then imported as STEP files into Abaqus as solid parts. Figure A.1 shows the import settings used.

The parts used can be seen in figure A.2. The bolts were used in both models, while the design spaces were different in each model. The bolts were simplified in order to save computing time. A washer was modeled together with the bolt to reduce the number of parts and subsequent interactions needed. The bolts were partitioned, as indicated on the lines on the parts in figure A.2 a) and b). These partitions were used for meshing and for applying loads and boundary conditions.

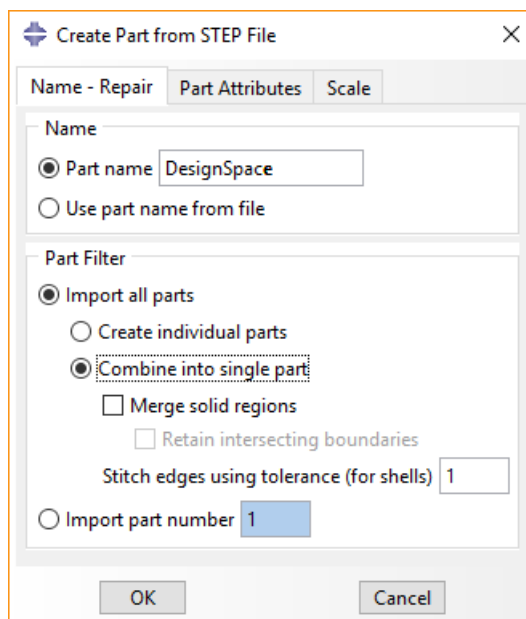


Figure A.1: Import dialogue box.

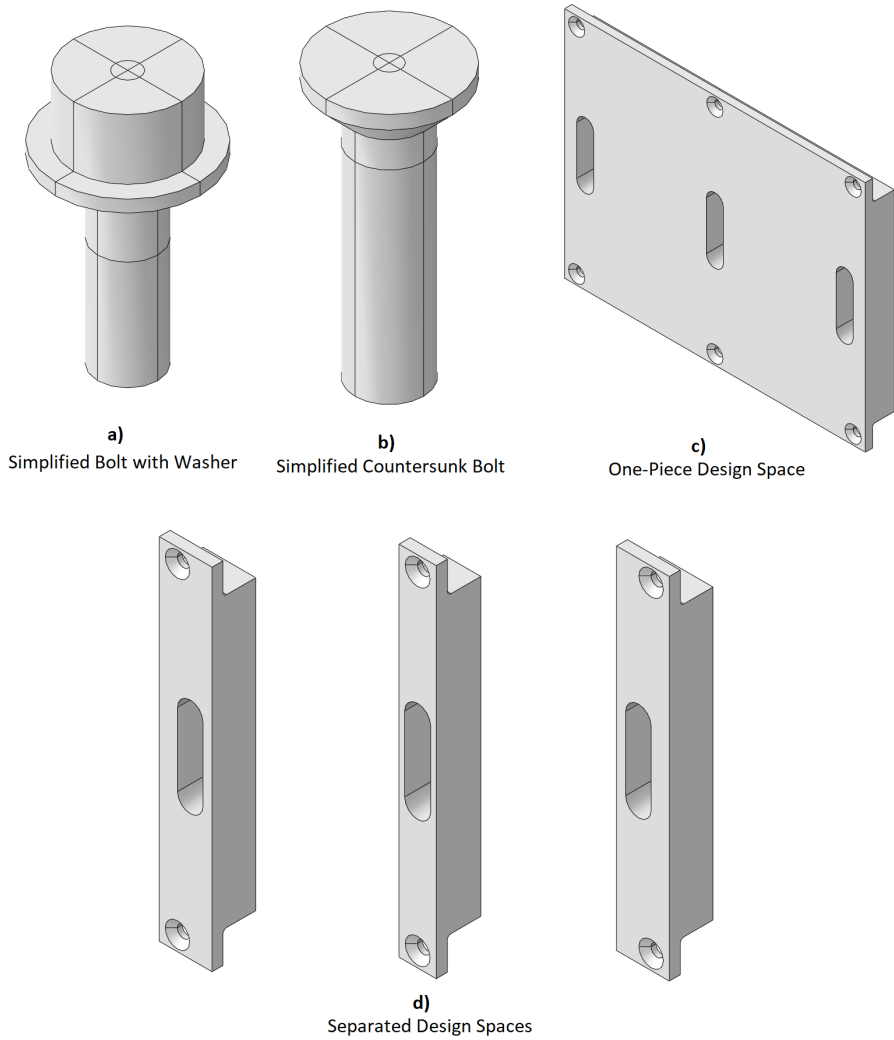


Figure A.2: Parts used in Abaqus.

A.2 Properties

The property environment is where the materials are defined and added to the parts. Two different materials were used, generic steel and AlSi10Mg. The material data for AlSi10Mg is summarized in table 5 in section 3.1.3. The inputted values are shown in figure A.4 and A.5. In Abaqus it is not possible to define units. However, relations between the units still exist, as seen in figure A.3. Because of this, the driving factor for which units are used for the properties and results is the unit used to model the parts. In this case, millimeters were used during modeling. As such, the density is entered in tonne/mm^3 and the Young's modulus and shear modulus uses MPa .

Quantity	SI	SI(mm)	SI	US Unit(ft)	US Unit(inch)
Length	m	mm	m	ft	in
Force	N	N	kN	lbf	lbf
Mass	kg	$tonne (10^3 kg)$	$tonne$	$slug$	$lbf s^2/in$
Time	s	s	s	s	s
Stress	$Pa (N/m^2)$	$MPa (N/mm^2)$	kPa	lbf/ft^2	$psi (lbf/in^2)$
Energy	J	$mJ (10^{-3} J)$	KJ	$ftlbf$	$inlbf$
Density	kg/m^3	$tonne/mm^3$	$tonne/m^3$	$slug/ft^3$	$lbf s^2/in^4$

Figure A.3: Overview of units relations in Abaqus.

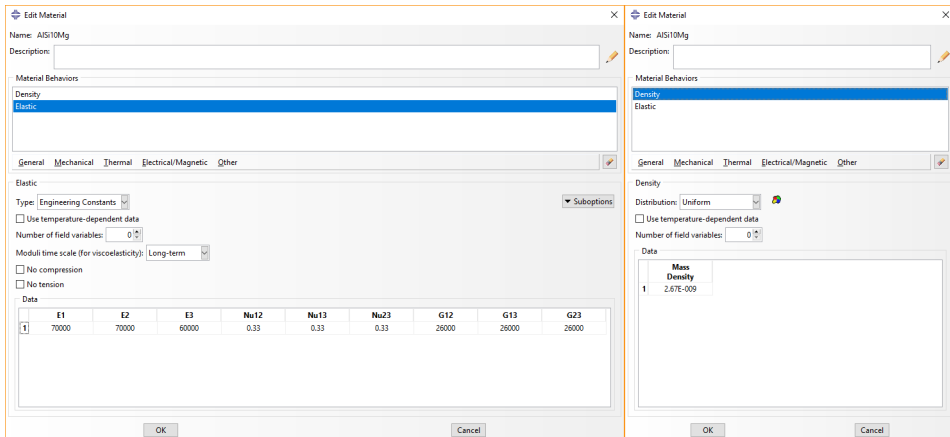


Figure A.4: Properties used for AlSi10Mg.

Because an orthotropic material model is used for AlSi10Mg, a material orientation is needed for the design space parts. This can be seen in figure A.6.

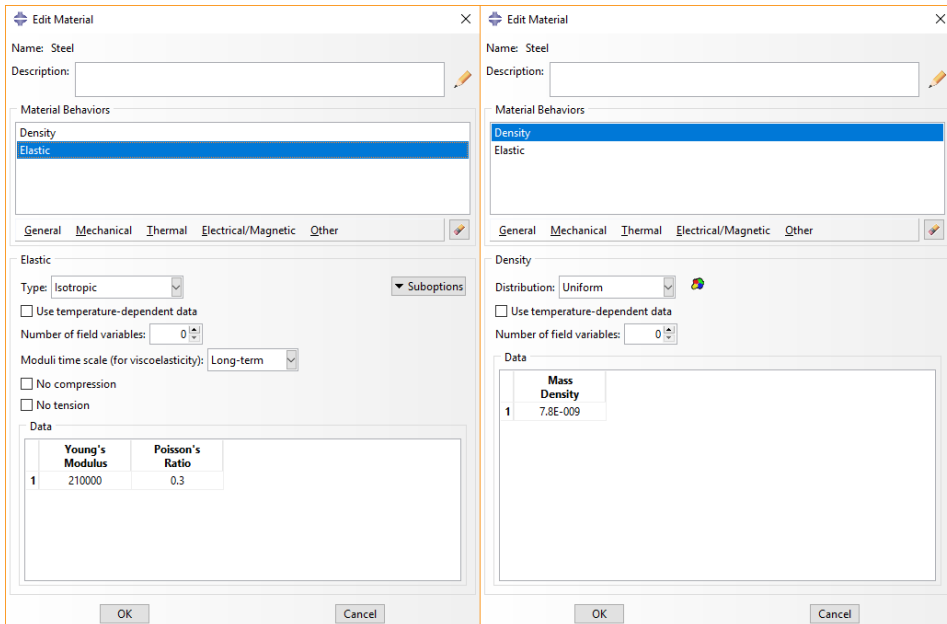


Figure A.5: Properties used for steel.

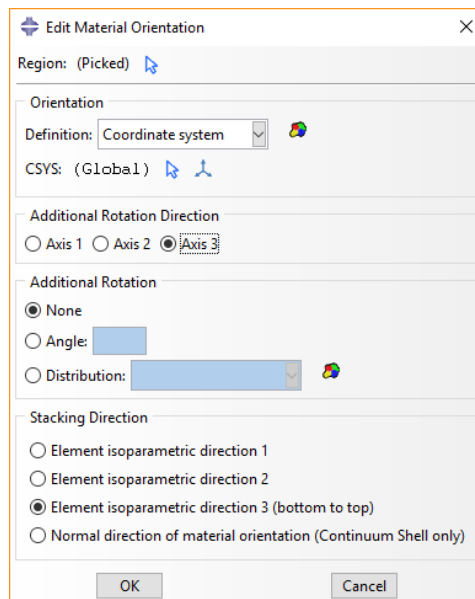


Figure A.6: Material orientation.

A.3 Assembly

In the assembly environment, instances are created from the parts defined earlier (figure A.7). The design space was added first, and then the bolts were positioned correctly using face to face and coaxial constraints. Only one of each of the different bolts were added initially. Linear pattern was then used to position the remaining bolts. The rear view of the final assembly of the one-piece design space can be seen in figure A.8.

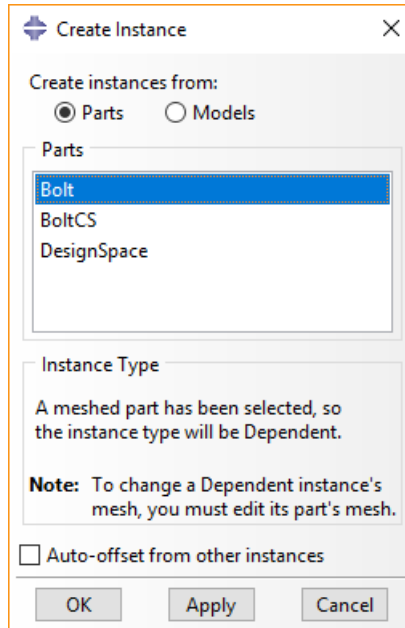


Figure A.7: Create instance.

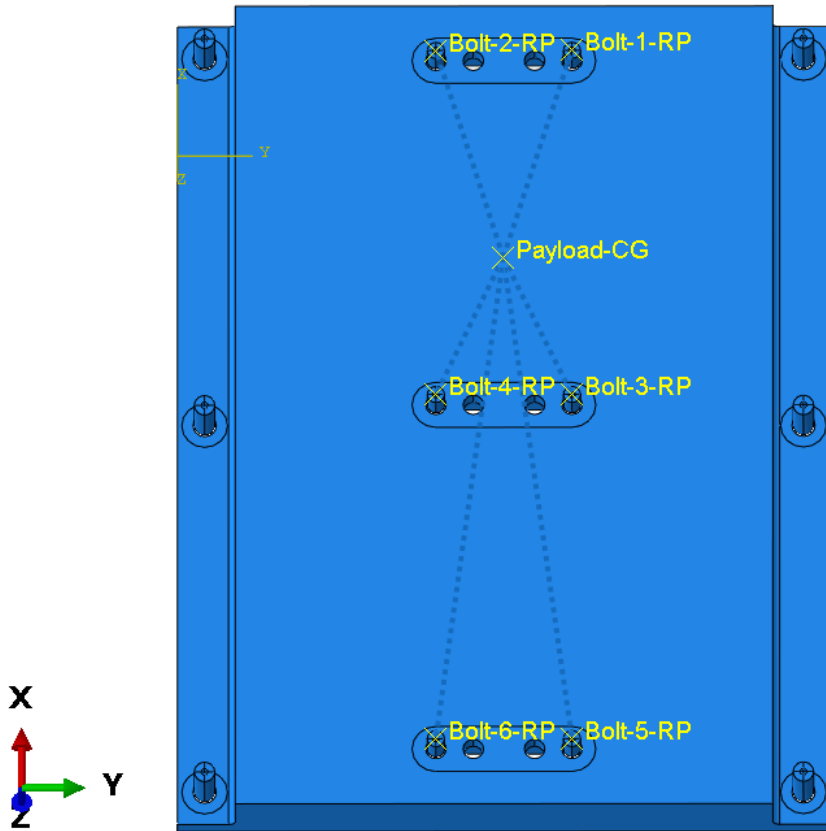


Figure A.8: Rear view of the assembly.

A.4 Step

Since each load case in this problem is independent of each other, linear perturbation steps are used. Figure A.9 shows how to create a linear perturbation step. One step is created for each load case, as seen in figure A.10.

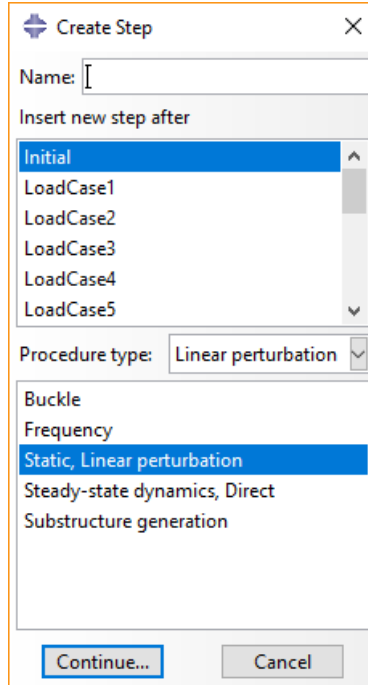


Figure A.9: Create linear perturbation step.

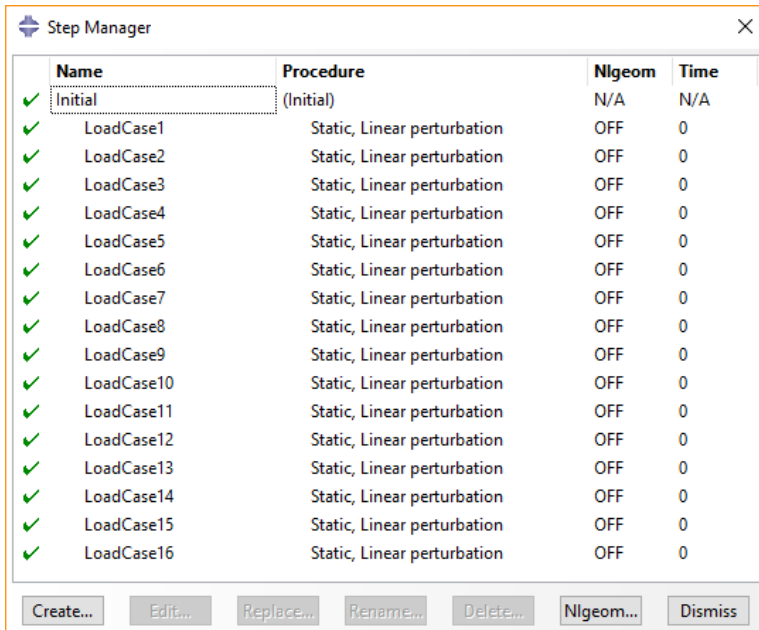


Figure A.10: Step manager.

A.5 Interaction

The interaction module is used to create constraints such as ties and couplings, as well as defining interactions between parts. The "find contact pair" function seen in figure A.11 was used to automatically find and create contacts between the bolts and the design space parts. Figure A.12 shows the different contacts in the model, while figure A.13 shows some of the settings used for each interaction. The figure also shows the master and slave surfaces. In general, the slave surface should have a finer mesh than the master surface to avoid errors or slow run times. Because of this, the design space was chosen as the master surface for all these interactions. The contact properties are shown in figure A.14. Instead of defining each contact pair separately, a general contact interaction could have been used. While this is simpler to set up, it also leaves the user with less control over the interactions.

During the initial simulations, "uncoupled regions" between the countersunk bolts and the design space was discovered. To solve this problem, a tie constraint was used on the contacting surfaces of these components. See figure A.15.

To model the connection between the payload CG and the bolts, connectors were defined. First, a reference point at the center of each bolt was created. Then, a wire feature was created from the payload CG to these reference points (figure A.16). Next, a connector section was created and assigned to the wires (figure A.17). For the connectors, "link" was used for the translation and "rotation" was used for the rotation. The link connector ensures that the distance between the two connecting nodes is constant and transfers axial loads. The rotation connector provides a rotational connection between the two nodes [19]. A connector type diagram can be seen in figure A.18.

Because a connector can only be applied between two nodes, a coupling constraint was defined between the reference point of the bolt and the "threads". A continuum distributing coupling was used, as seen in figure A.19.

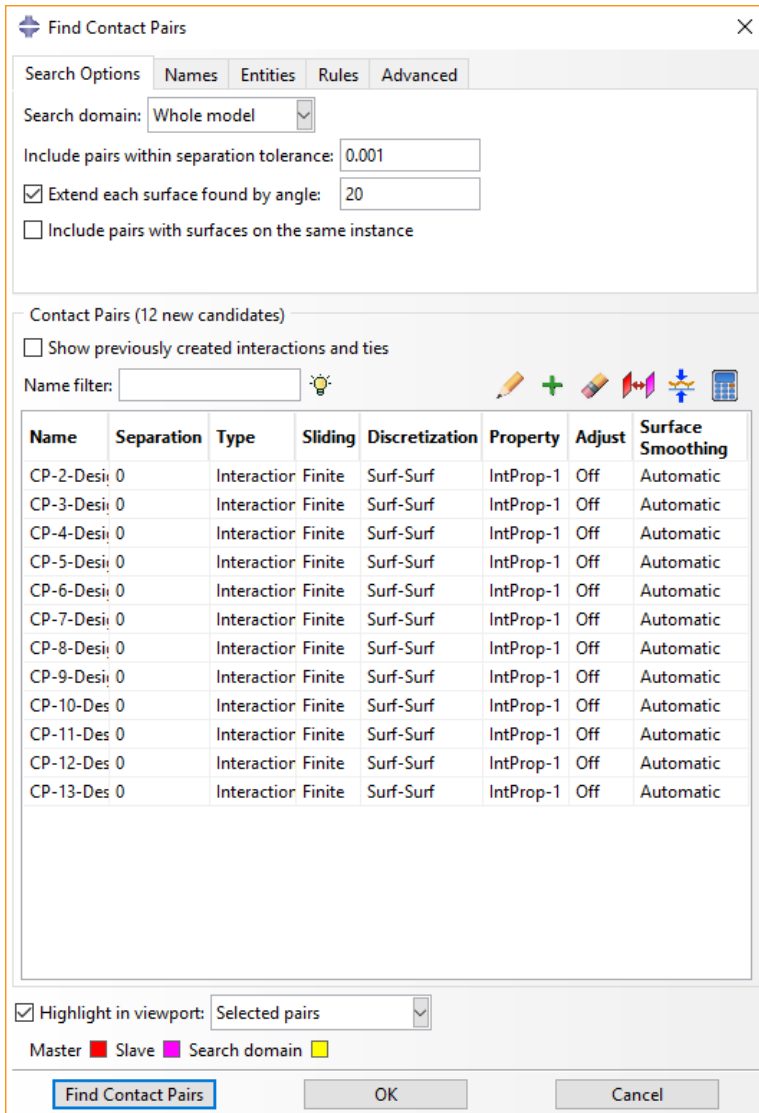


Figure A.11: Find contact pairs.

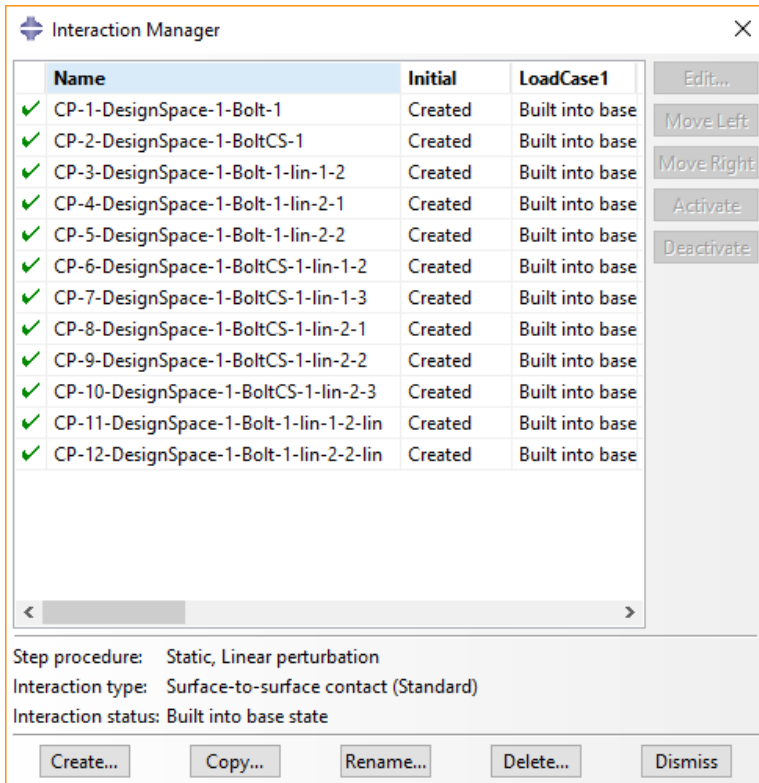


Figure A.12: Interaction manager.

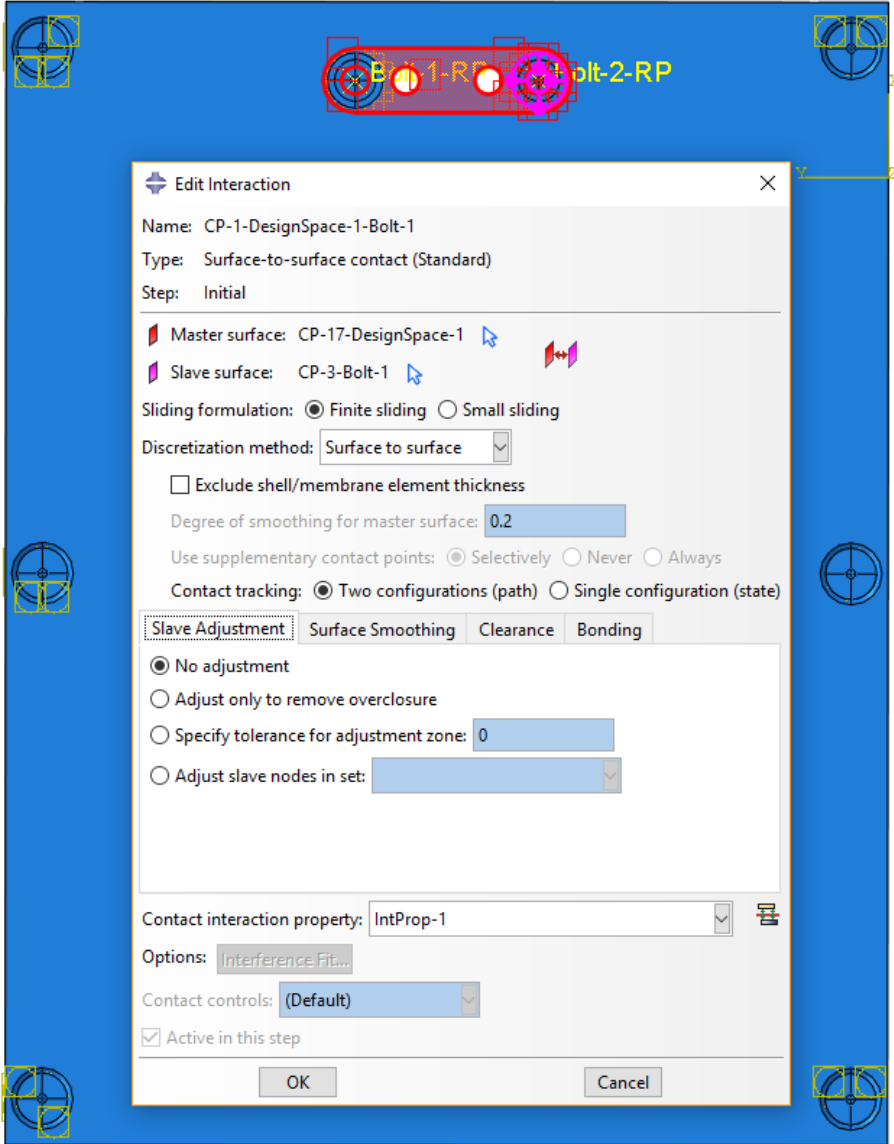


Figure A.13: Interactions with master and slave surfaces.

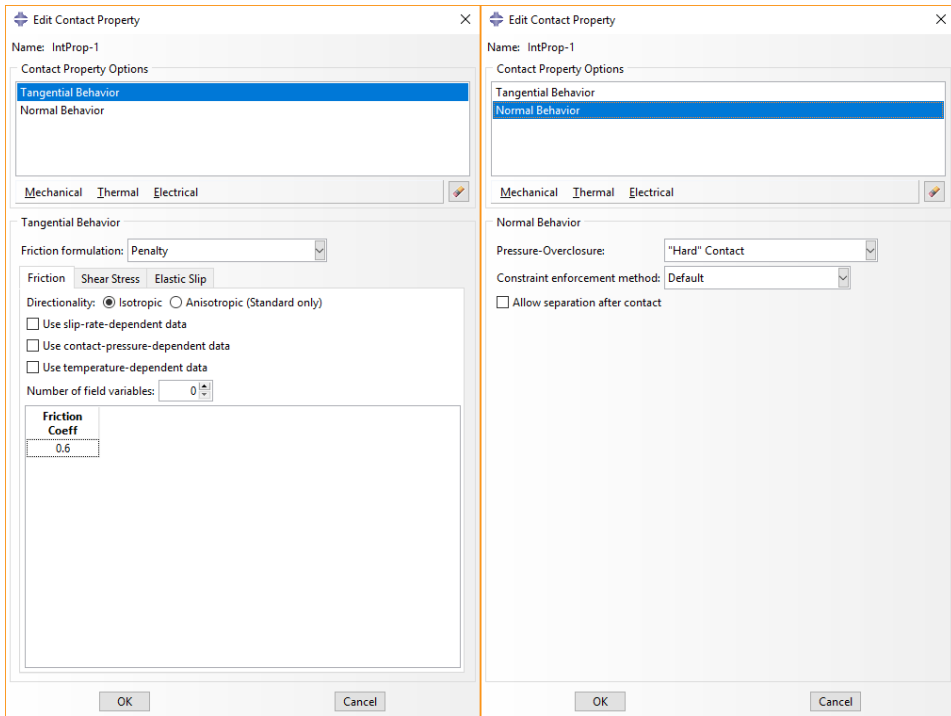


Figure A.14: Contact properties.

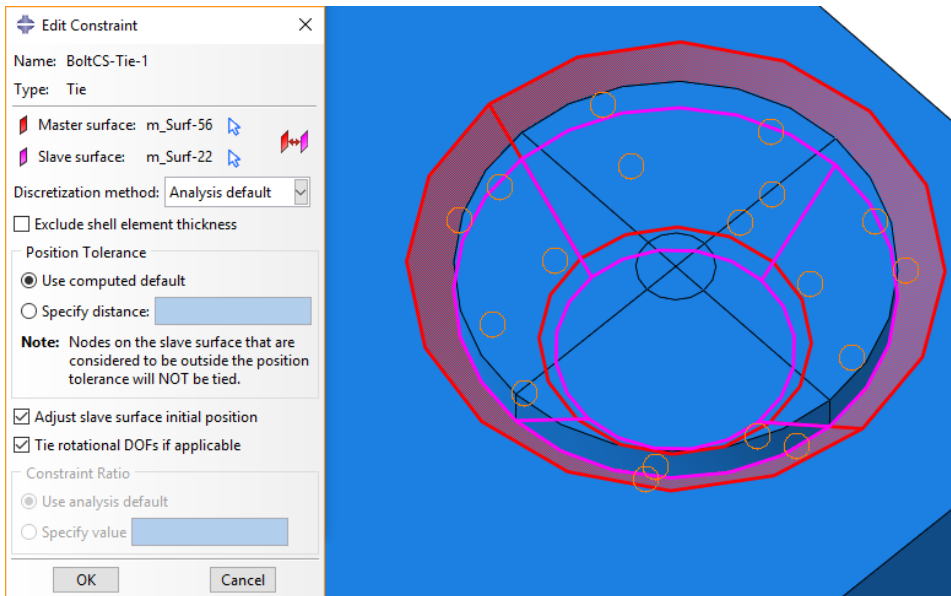


Figure A.15: Tie between the countersunk bolts and the design space.

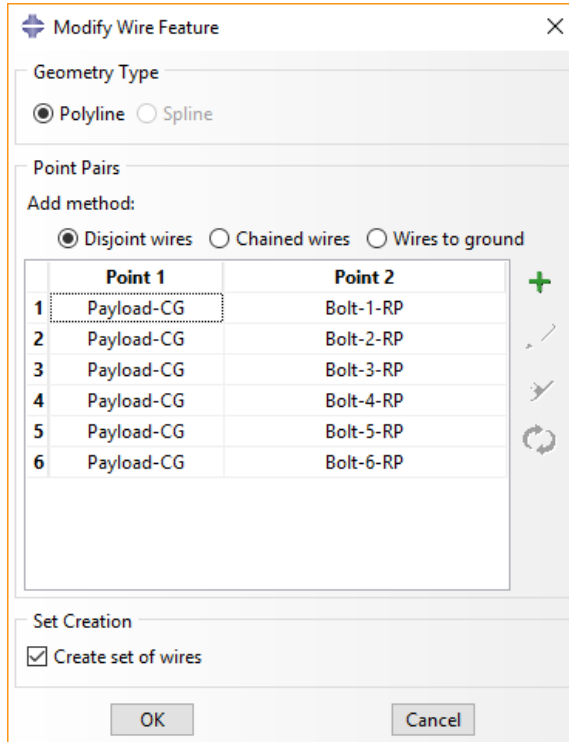


Figure A.16: Creating the wire feature.

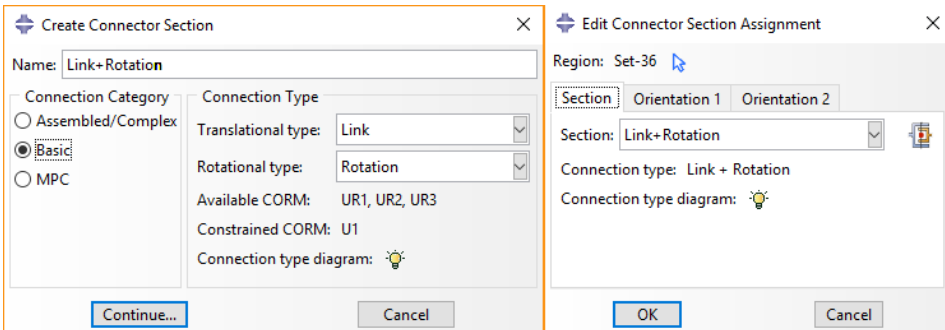


Figure A.17: Connector section creation and assignment.

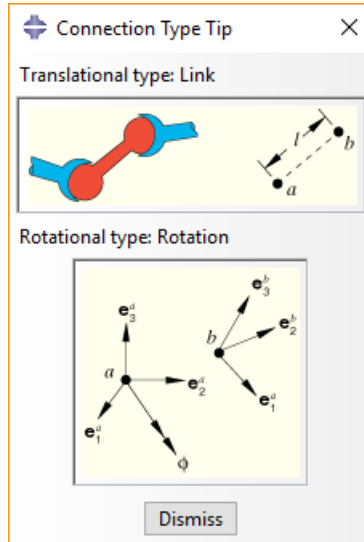


Figure A.18: Diagram of the connector properties.

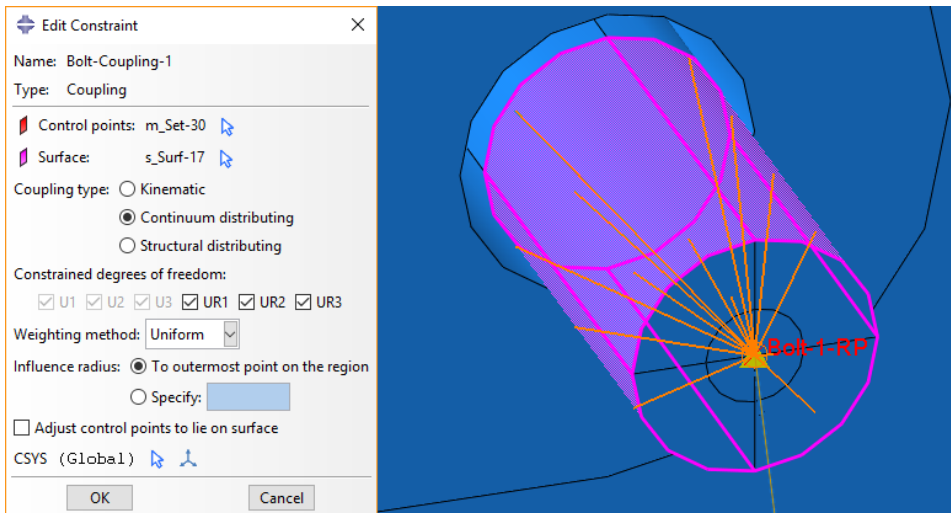


Figure A.19: Bolt coupling.

A.6 Load

The loads used are defined in table 4 in section 3.1.2. The loads were defined as concentrated forces on the payload CG, seen for load case 1 in figure A.20. The unit for forces is Newton. As described in section A.4, each load case is defined as its own step. This can be seen in the load manager in figure A.21.

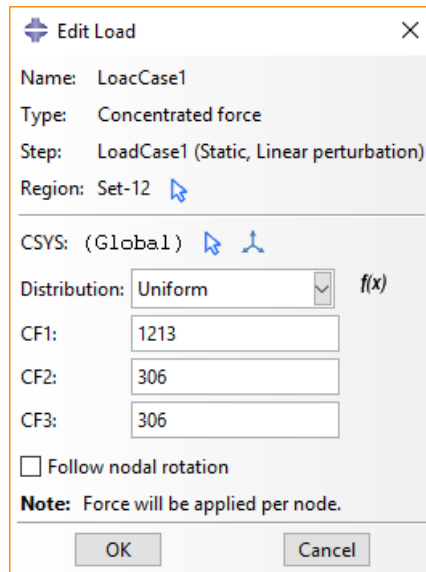


Figure A.20: Load case 1 [N].

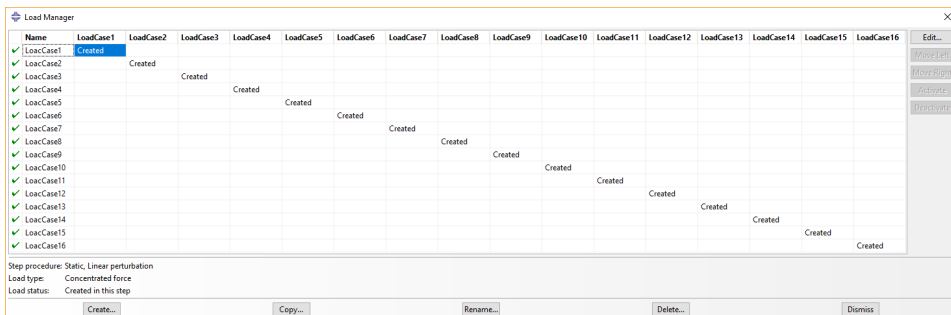


Figure A.21: Load manager showing the load cases (vertical) and steps (horizontal).

Because of the partitioning of the bolts, the boundary conditions and load are only applied to the threads of the bolts that are extended beyond the design space. For the boundary conditions, the surfaces of the threads of the countersunk bolts are encastred (figure A.22).

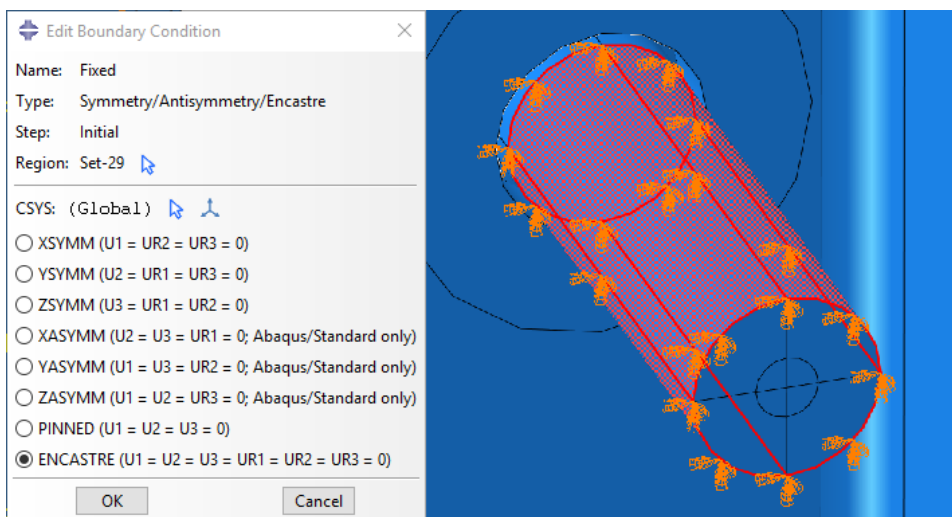


Figure A.22: Boundary conditions.

A.7 Mesh

A.7.1 Bolts

The mesh used for the bolts can be seen in figure A.23. The elements shapes were a combination of structured hexahedrons (green) and wedge (yellow) elements (figure A.24). This was possible due to the partitioning of the bolts. The mesh was made of 20-node quadratic brick elements, with reduced integration (C3D20R). The element size was 0.5 mm with curvature control of 0.1. Figure A.25 shows the full settings used for the mesh.

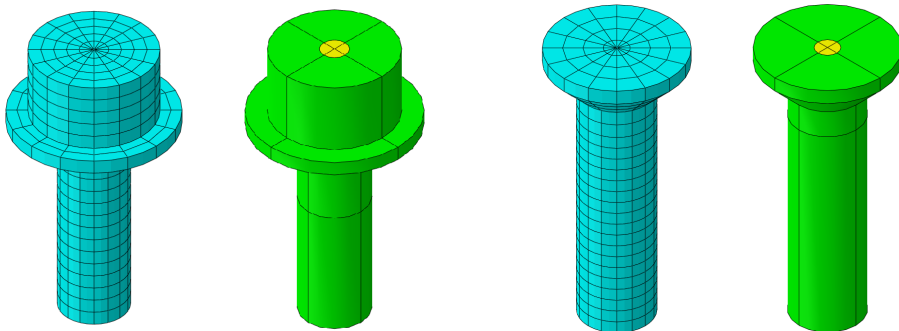


Figure A.23: Bolt mesh and sections.

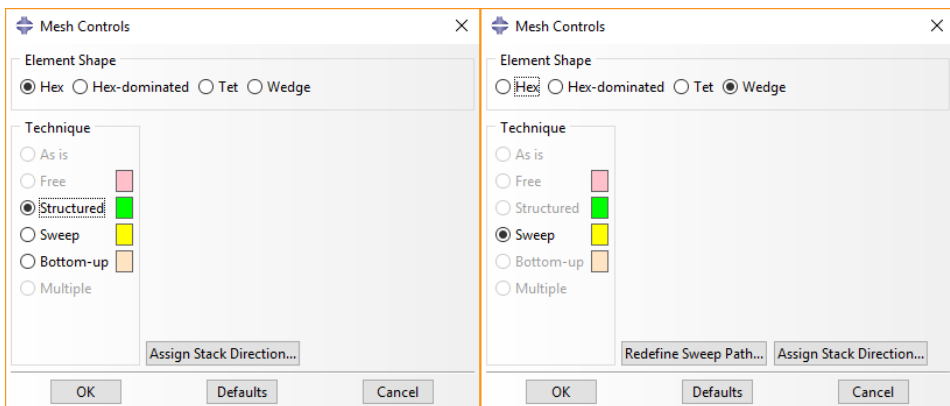


Figure A.24: Mesh controls used for the bolts.

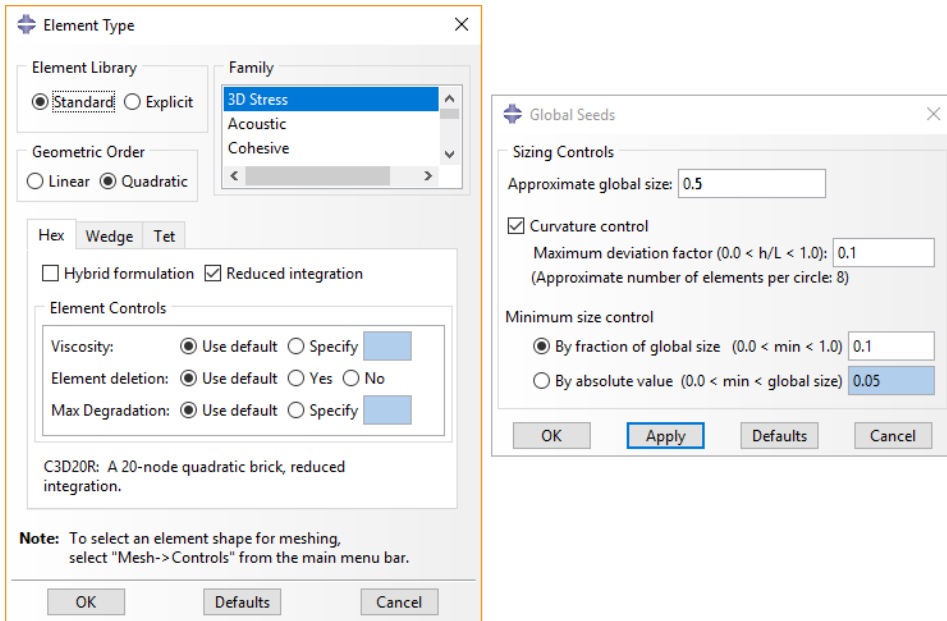


Figure A.25: Settings used for the bolt mesh.

A.7.2 Design Space

The design space mesh can be seen in figure A.26, and the settings used in figure A.27. The mesh consists of 10-node quadratic tetrahedrons with a free structure. The size of the elements was 1 *mm* with curvature control of 0.1.

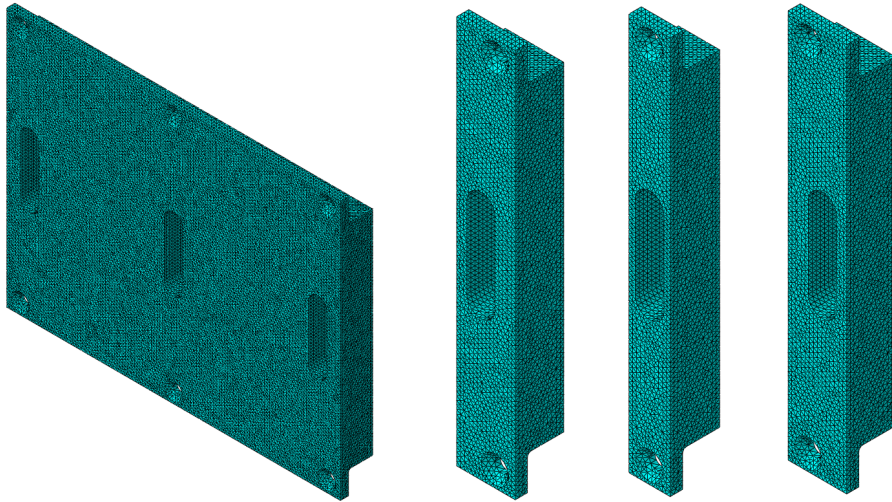


Figure A.26: Design space mesh.

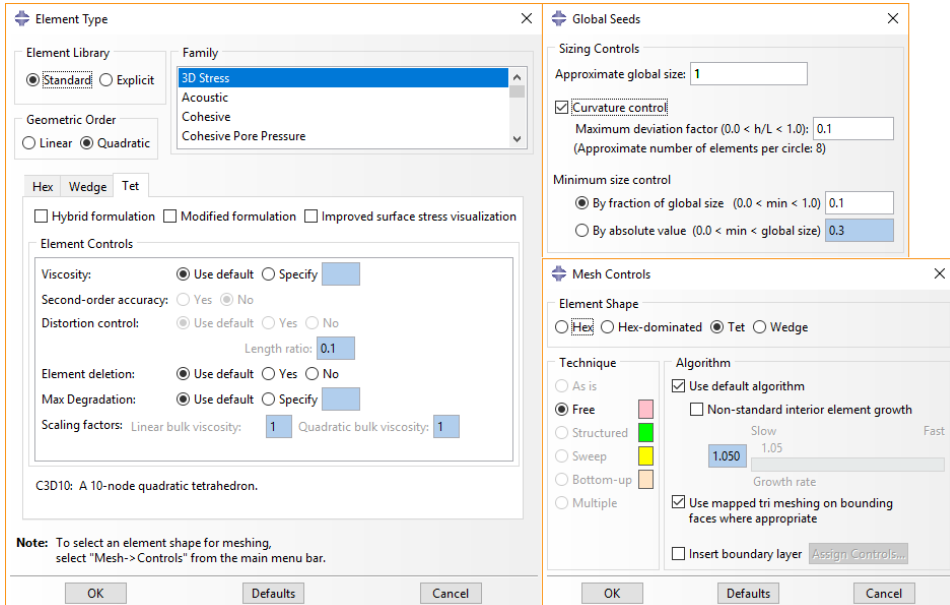


Figure A.27: Settings used for the design space mesh.

A.8 Optimization

The workflow for the optimization setup can be seen in figure A.28. For the optimization, a sensitivity-based process with a penalization factor of 3 has been established. The active region for the optimization process is only the design space. Two design responses were created: strain energy and weight, which can be seen in figure A.29. Because multiple linear perturbation steps are used, all these steps have been selected as active for the strain energy. The whole model has been selected as the region for the strain energy. Just the design space has been selected for the weight, as the weight calculated should not include the bolts.

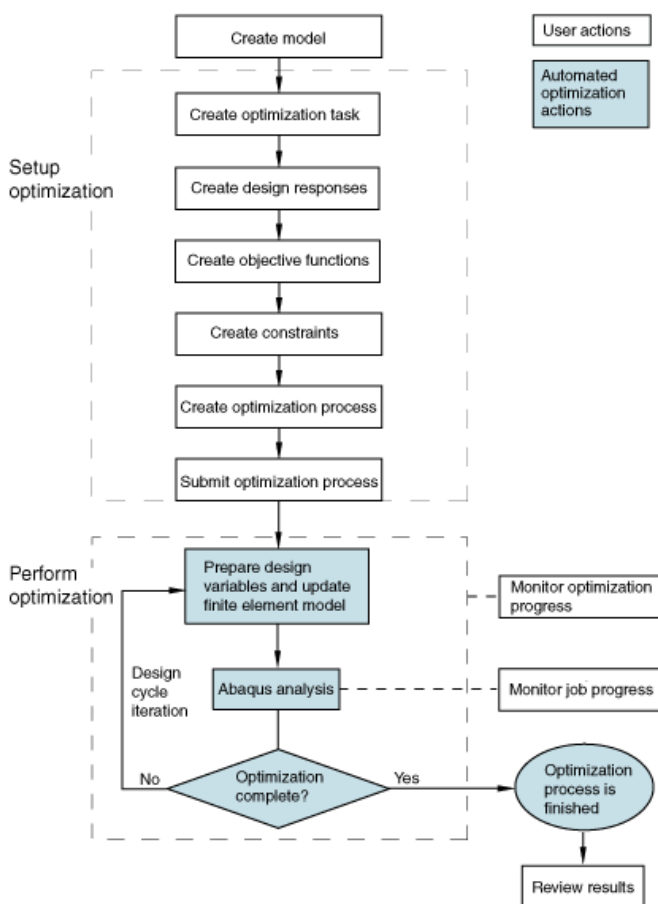


Figure A.28: Optimization process workflow [19].

The objective function is to minimize the strain energy (figure A.30a), and the optimization constraint is a weight lower or equal to 36 g (figure A.30b). The unit

for the weight is tonne.

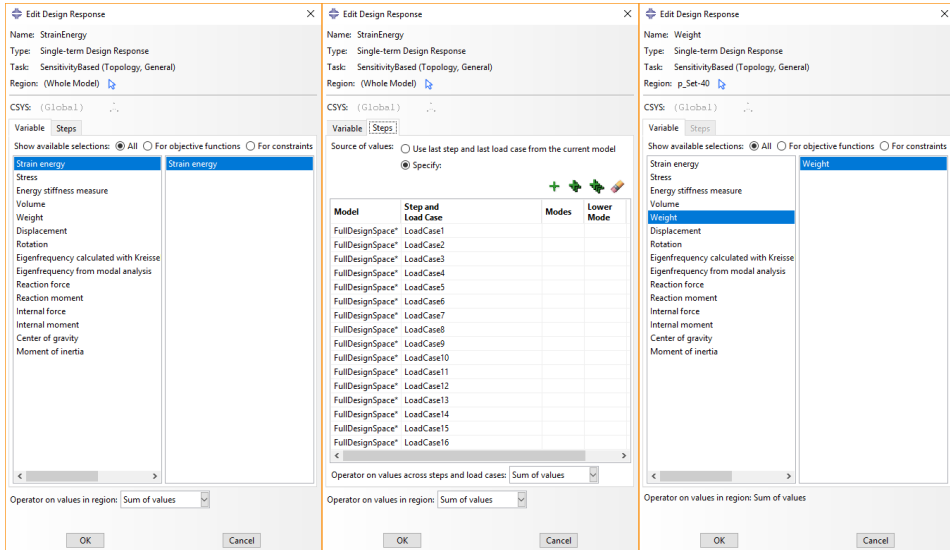
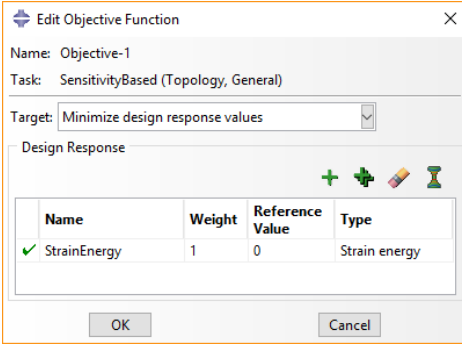
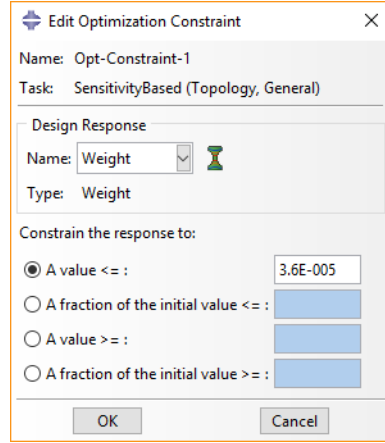


Figure A.29: Design responses.

The areas around the bolt holes, as well as the areas between the middle holes, have been selected as frozen areas, seen in figure A.31. These areas will therefore remain constant throughout the optimization process.



(a) Objective function.



(b) Optimization constraint [tonne].

Figure A.30: Objective function and constraint for the optimization.

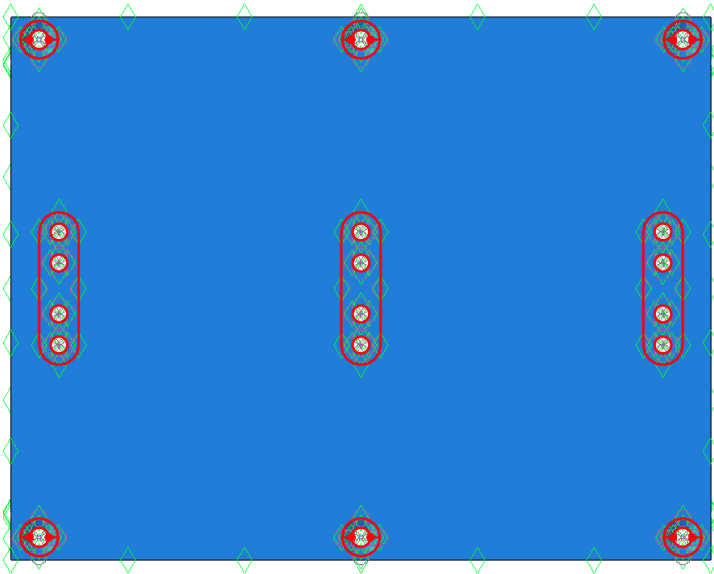


Figure A.31: Frozen areas.

B Post-Processing

This section shows more detailed figures from the post-processing process described in section 3.2. The same procedure was followed for all parts.

As described, after the results are extracted from Tosca, with smoothing and filtering cycles, the STL file is imported into Fusion 360. A quarter of the model is then cut out. The quarter in the top right corner of figure B.32 was used for this. However, due to automatic smoothing of sharp edges because of the T-spline body used in the later steps, an offset of 2 *mm* away from the symmetry planes was used (figure B.33 This effect can be seen in figure B.34. Without an offset, the subsequent mirror operations would have yielded poor results, or even failed. The extra material due to the offset was removed again after the model was converted to a solid body.

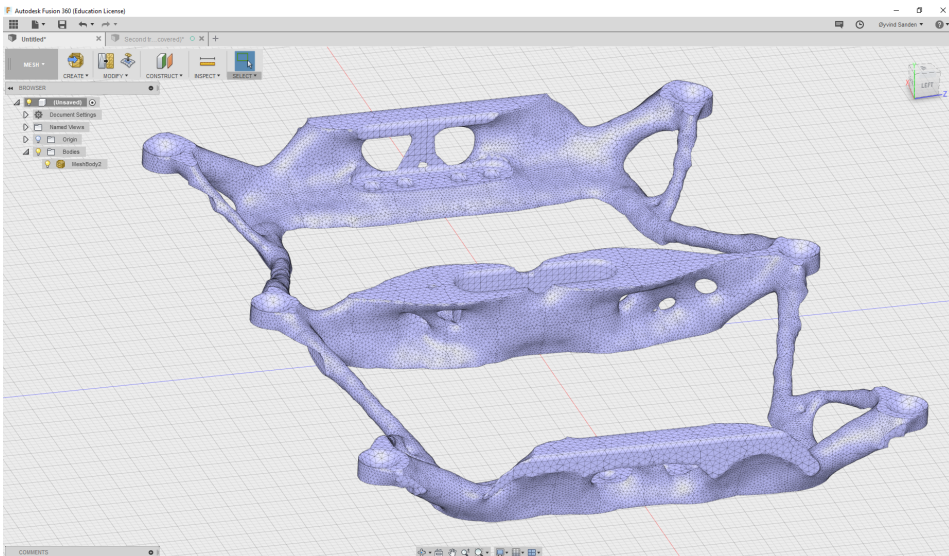


Figure B.32: STL file imported into Fusion 360.

The smoothing operations seen in figure B.35 and B.36 were done with a smoothing factor of 1. Most of the jagged edges were removed this way. Figure B.37 shows how excessive smoothing effectively shrinks thin member. This figure was created using a smoothing factor of 17 to demonstrate this effect.

Figures B.38 and B.39 shows the settings used for conversion to OBJ and then to a T-spline body. Figure B.40 shows the T-spline body after conversion. The T-spline body is made up of a number of control points that form edges and faces between each other. All of these vertices, edges, and faces can be edited, which gives the user much better control over the shape than by editing a mesh body. In

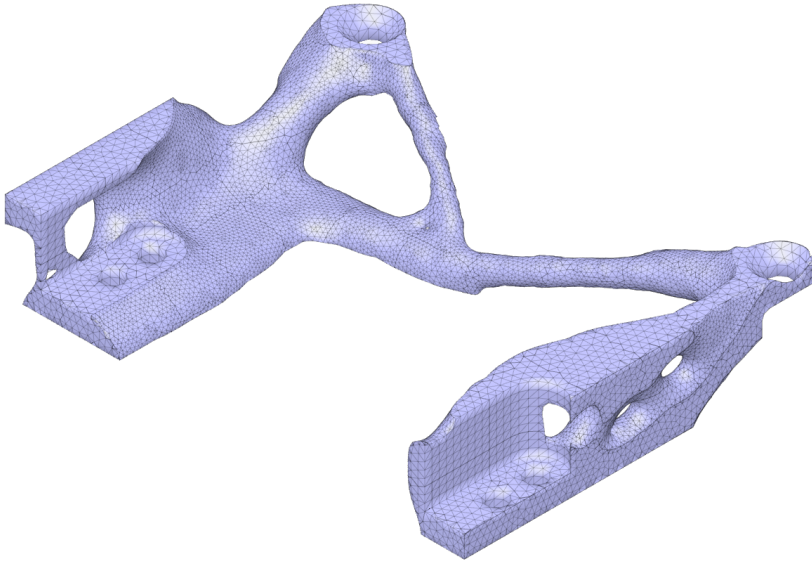


Figure B.33: Quarter of the mesh body.

Fusion, the body is edited by using the "Edit Form" feature. This feature has three transform modes: translation, rotation, and scaling. The handle seen in figure B.41 is used to control the transformation either by dragging or by entering numerical values. Figure B.42 shows the result before and after using this feature to edit the top edge of the top/bottom brackets.

Figure B.43 show the difference between the mesh body (blue) and the T-spline body after editing. Some of the difference comes from active editing using Edit Form, but a general smoothness also comes from the T-splines naturally.

After the body was converted to a solid (figure B.44 and B.45), it was imported into NX. The surrounding areas around the bolt holes, along with the excess material from the symmetry offset, were first cut out using subtractive extrusion operations. The areas around the bolts were then extruded back to the model with the right dimensions. The bolt holes were then added using the hole feature. Finally, the model was completed by mirroring the body across the two symmetry planes. The finished model in NX can be seen in figure B.46 All the dimensions were based on the position of the model origin which remained through all the conversions. These operations can be done in any CAD program.

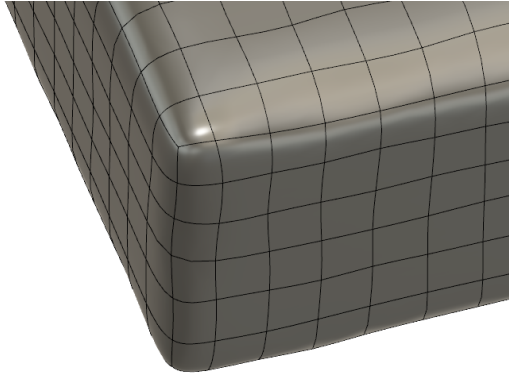
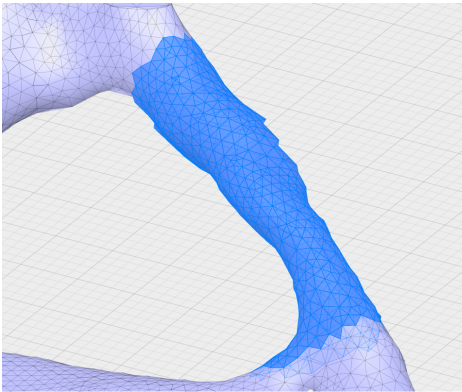
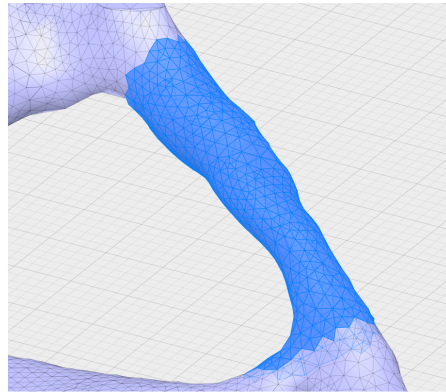


Figure B.34: Smooth edges because of the T-spline body.

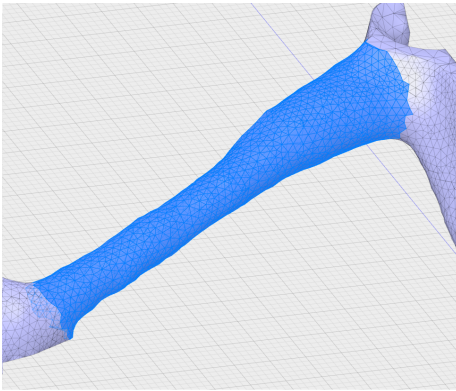


a) Before Smoothing

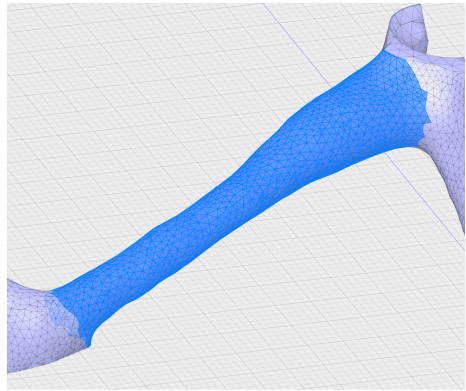


b) After Smoothing

Figure B.35: Before and after smoothing.



a) Before Smoothing



b) After Smoothing

Figure B.36: Before and after smoothing.

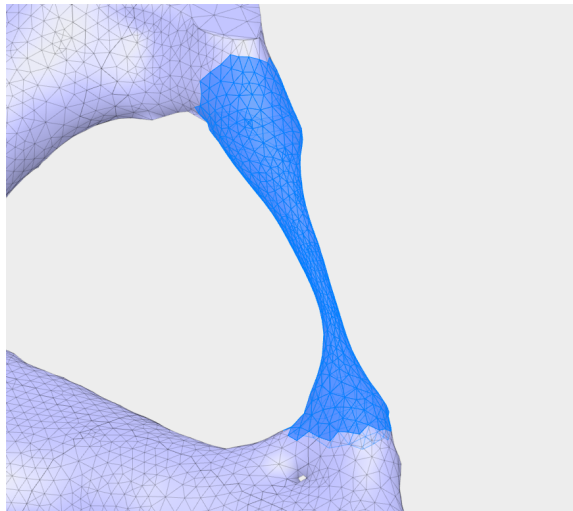


Figure B.37: Result after excessive smoothing.

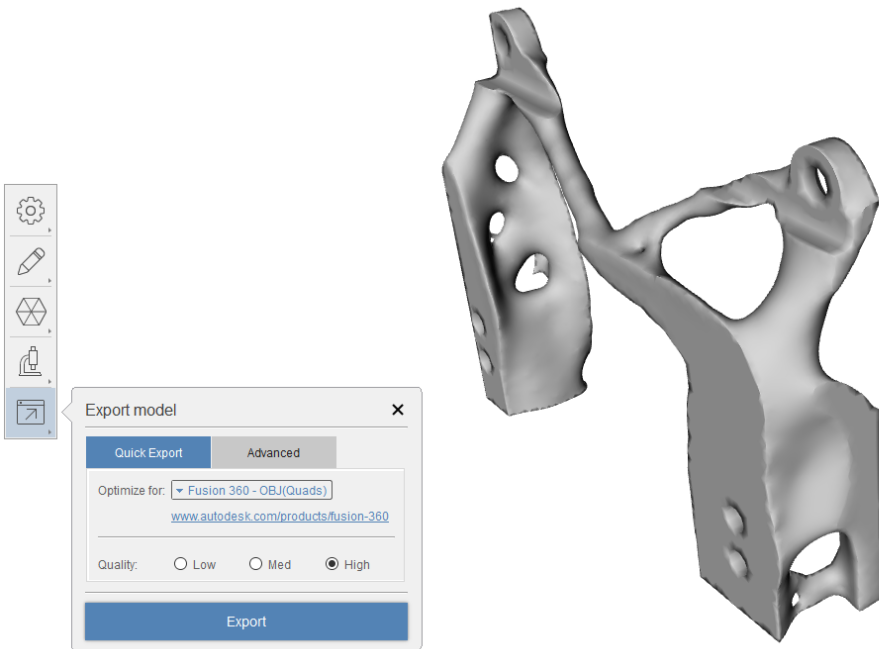


Figure B.38: Exporting to an OBJ file in ReCap.

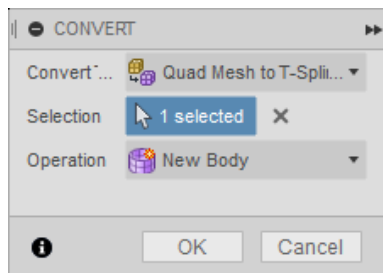


Figure B.39: Converting from mesh to a T-spline body.



Figure B.40: Converted T-spline body.

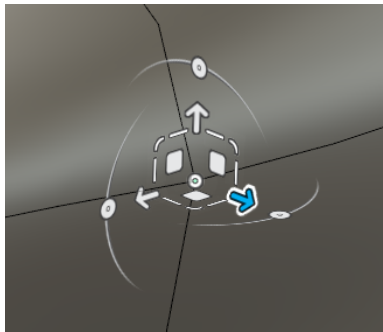


Figure B.41: The handle used to edit the T-spline body.

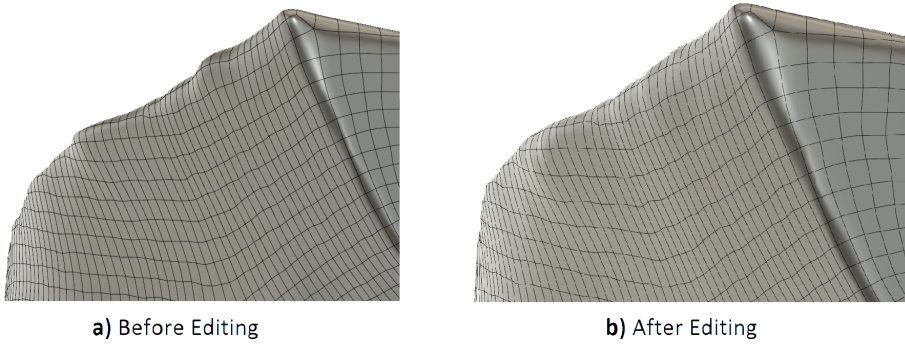


Figure B.42: Before and after editing the the top edge of the T-spline body.

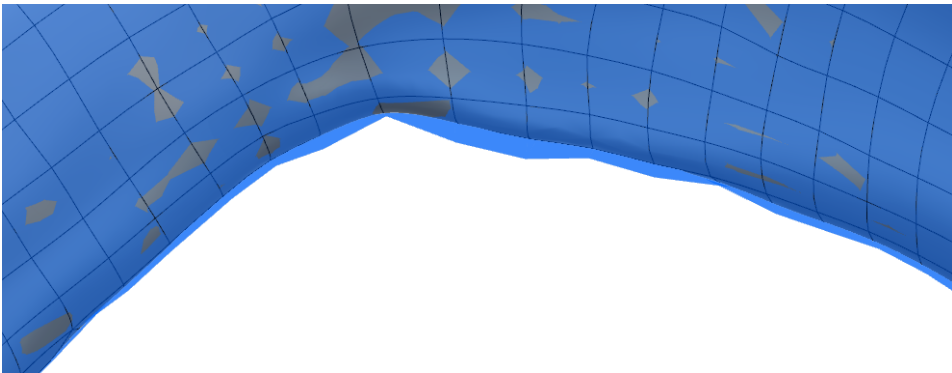


Figure B.43: The difference between the T-spline body (gray) and mesh body (blue)

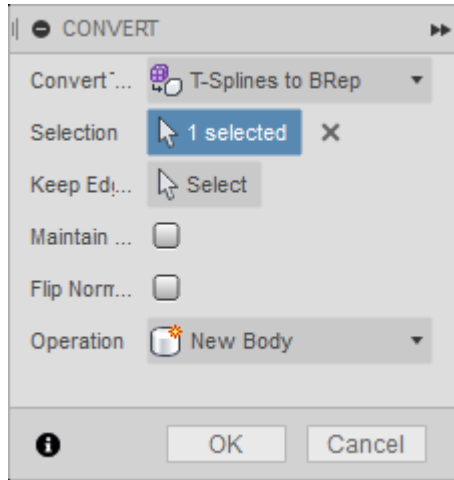


Figure B.44: Converting from a T-spline body to a solid body.

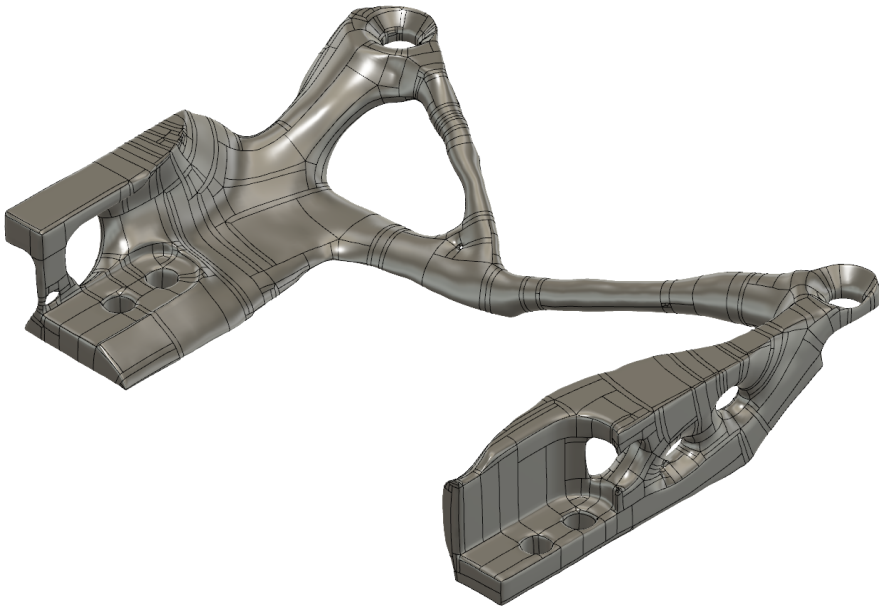


Figure B.45: Converted to a solid body (BRep).

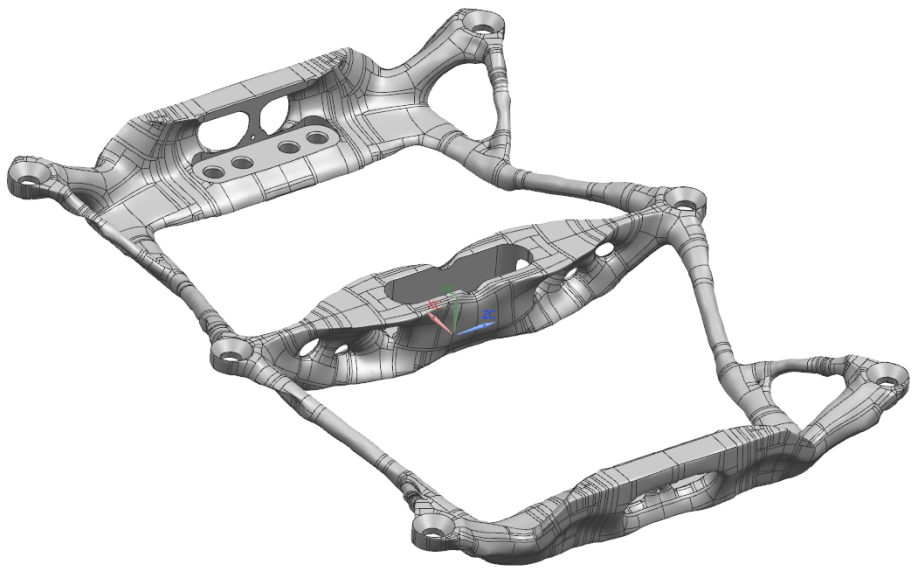


Figure B.46: The finished body in NX.

C Previous Models

This appendix covers some of the previous models used in this project.

The first model that was set up can be seen in figure C.47. In this model, the complete satellite assembly was set up to try to model how the surrounding components would interact with the design space. However, this model presented several challenges. Firstly, the model was very large, which meant that a lot of computing time would be needed. The initial attempt to reduce the computational time was to use a symmetric assembly, as seen in figure C.48. The second challenge with this model was the only CAD files that were available at the time were the payload and antenna assemblies. The other components were modeled mainly using reference pictures found on the Internet. This meant that the size of the components, as well as the materials and the connection to other components, was very uncertain. The final challenge with this model was how to apply the loads correctly. At first, the loads were applied on the outside of the panels as pressure, seen in figure C.49.

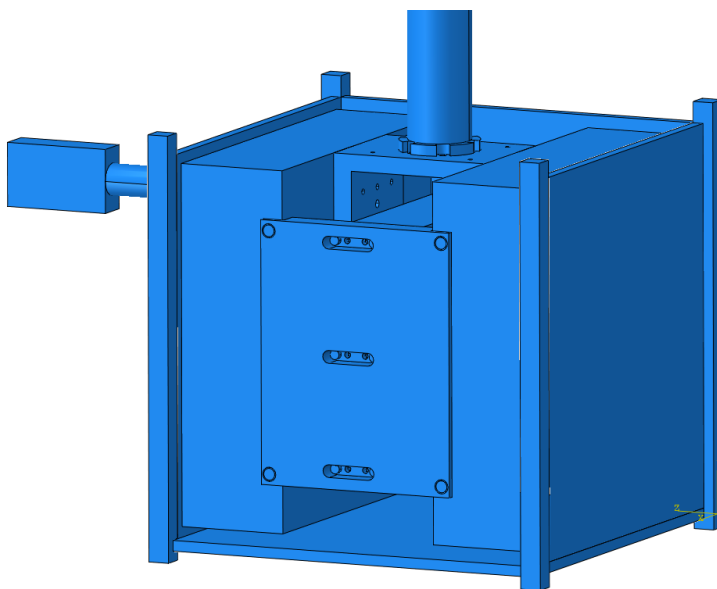


Figure C.47: Full satellite assembly with the top and side panels removed.

In the next model, only the design space and accompanying bolts were added, seen in figure C.50. This model was very similar to the one described in section 3.1.4, but at this point the design space was not made symmetric yet. For this model, the material used was Ti6Al4V. The results from a condition-based algorithm after 30 cycles can be seen in figure C.51. Note that the stresses are calculated with an averaging of 75 %. Compared to the results in section 4.1, the members are much thinner and the result is not "symmetric". The thin members are both a

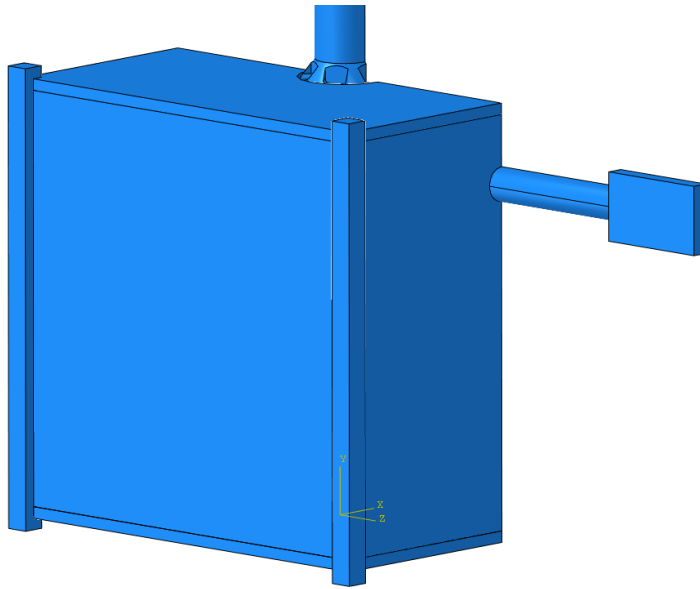


Figure C.48: Symmetric satellite assembly.

product of the condition-based algorithm, as discussed in section 1.3.1, and also from the increased stiffness of the titanium compared to aluminum. When looking at the history of the optimization process, it was revealed that the algorithm only removed the material on the right side in the final iterations. The result after 22 design cycles can be seen in figure C.52. At this point, the weight of the part was ca. 67 g, while the finished result after 30 cycles was 42 g. The weight target was still 36 g. This was an indication that the volume available for the optimization process was not enough to create a symmetric result. It was then decided that the design space would be changed slightly to achieve symmetry. The material was also changed from titanium to aluminum to get more available volume because of the lower density of aluminum. By using aluminum, the comparisons with the original parts would also be more "real", as the potential increased performance of the parts would only come from the new topology of the parts, and not from the material used.

In another earlier attempted version of this model, the boundary conditions were slightly different. The surrounding system of the payload was not symmetrical due to the magnetometer, seen on the left side of figure C.47, and this could affect the behavior of this system. The center of gravity of this system was calculated using the already modeled parts. This point can be seen in figure C.50 as the reference point "System-CG". Similarly to the connections from the payload CG, this point was connected to the countersunk bolt in the corners of the design space. The system CG was then constrained as fully fixed. However, this new boundary

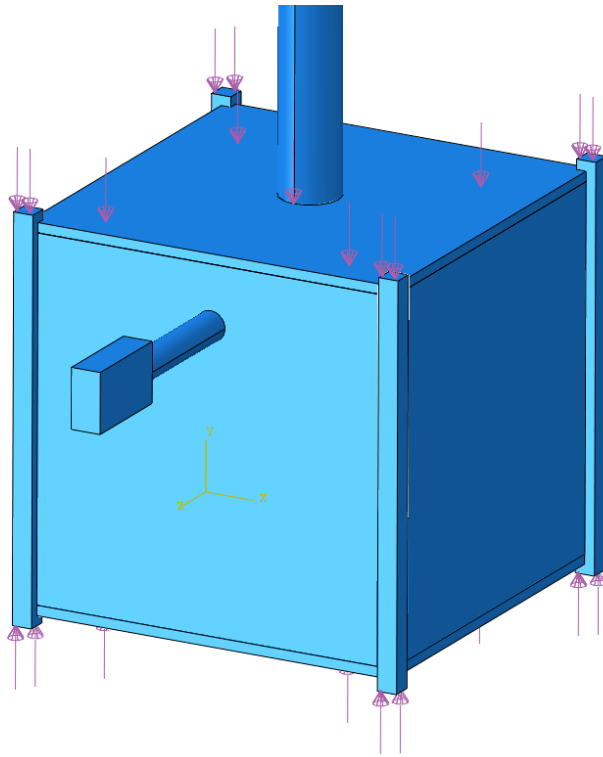


Figure C.49: Load applied to the satellite assembly.

condition caused numerical singularities in the following analysis. The boundary conditions were subsequently changed to fix the threads of the bolts instead.

After the design space was made symmetric, the next model that was used was a quarter of the design space, seen in figure C.53. Symmetric boundary conditions were used on the surfaces along the symmetry planes, as well as on the payload CG in order to prevent rigid body motion between the CG and the bolts. The problem with this approach was that by restricting the motion of the CG, the loads that worked in these directions were canceled out. This model was then changed to a full design space, as described in section 3.1.4.

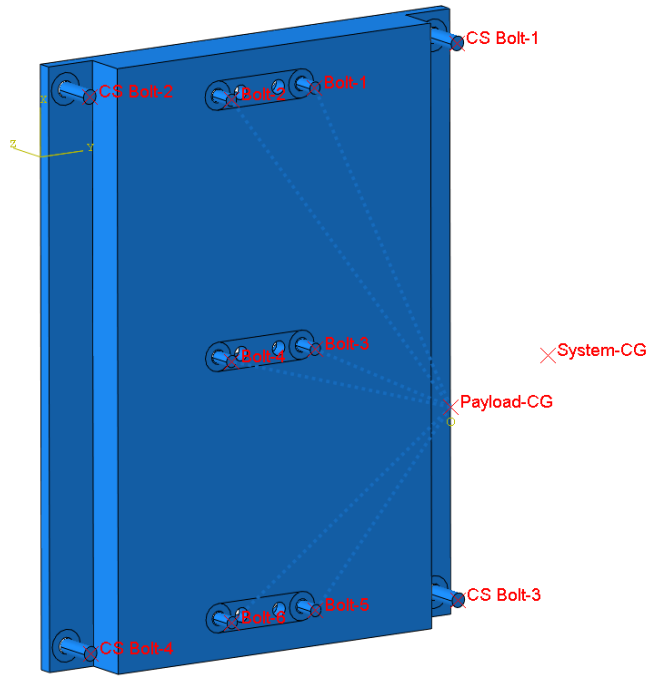


Figure C.50: The complete design space before it was made symmetric.

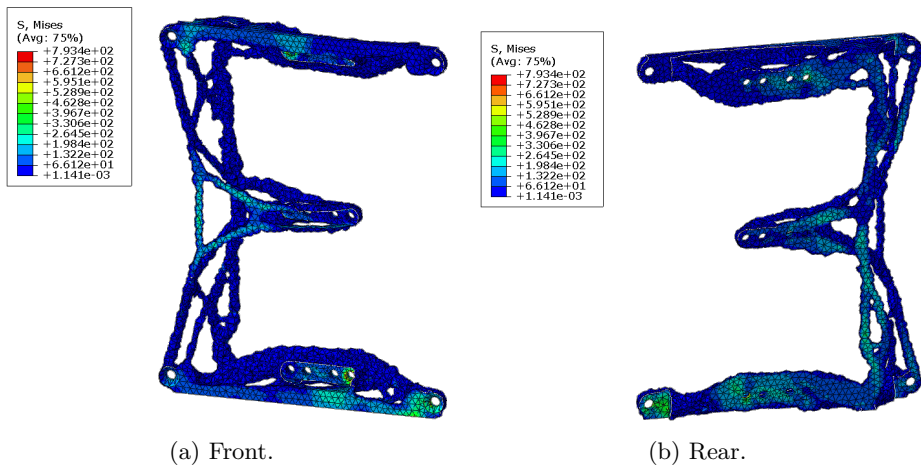


Figure C.51: Front and rear view of the results with titanium.

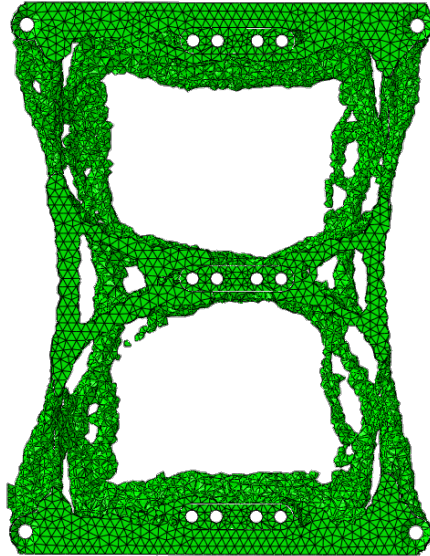


Figure C.52: Result after 22 cycles.

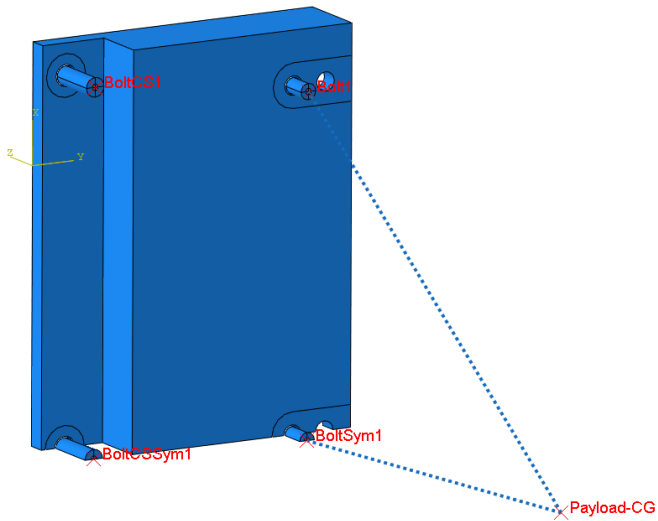


Figure C.53: Quarter model.

D Matlab Code

```
1  clc
2  clear variables
3  close all
4
5  E = 70e9; %Pa
6  rho = 2700; %kg/m^3
7
8  l = [20 30 40 50]*1e-3; %m
9
10 d = [1:10]*1e-3; %m
11
12 omega = zeros(length(l),length(d));
13
14 for i = 1:length(l)
15     omega(i,:) = pi*d/(8*l(i)^2)*sqrt(E/rho);
16
17     hold on
18     plot(d,omega(i,:), 'DisplayName', 'test')
19
20 end
21
22 xlabel('Diameter [m]')
23 ylabel('Frequency [Hz]')
24 legend({'L = 20 mm', 'L = 30 mm', 'L = 40 mm', 'L = 50 mm'
        }, 'Location', 'northwest')
```


E Arianespace Auxiliary Passengers User's Manual

Selected pages.

MICRO AUXILIARY PASSENGER DESIGN AND VERIFICATION REQUIREMENTS

Chapter 4

4.1 Introduction

The design and dimensioning requirements that shall be taken into account by any Customer intending to launch a Micro Auxiliary Passenger compatible with the Arianespace Systems are detailed in this chapter.

4.2 Design Requirements for Micro Auxiliary Passenger

4.2.1 Safety Requirements

The Customer is required to design the spacecraft in conformity with the CSG Safety Regulations, refer to the Payload Safety Handbook, CSG-NT-SBU-16687-CNES, Edition 1, Revision 1 dated 06 May 2015.

4.2.2 Selection of spacecraft materials

The spacecraft materials must satisfy the following outgassing criteria:

- Total Mass Loss (TML) $\leq 1 \%$;
- Collected Volatile Condensable Material (CVCN) $\leq 0.1 \%$.
measured in accordance with the procedure "ECSS-Q-70-02A".

4.2.3 Micro S/C Mass Properties

- The mass of a Micro Auxiliary Passenger must be in the range from **50 to 200 kg**.
- Center of gravity position:
 - $X_G < 450 \text{ mm}$ (from the mounting plane of the spacecraft)
 - The static unbalance of the spacecraft must stay within $d \leq 15 \text{ mm}$

For satellites with characteristics outside these domains, please contact Arianespace.

NOTE1: Large CoG offset can be counteracted by an adequate tuning of the separation system when off-the-shelf adapter is used. Refer to separation system description in Annex 2.

NOTE2: The dispersion on the CoG offset shall be no more than 3 mm at the time of Final Mission Analysis Kick-off.

4.2.4 Frequency Requirements for Micro Auxiliary Passenger

To prevent any dynamic coupling with fundamental modes of the Launch Vehicle and Carrying System, the Micro Auxiliary Passenger shall be designed with a structural stiffness which ensures that the following requirements are fulfilled. In that case, the design limit loads given in next paragraph are applicable.

Lateral frequencies

The fundamental frequency in the lateral axis of a spacecraft hard-mounted at the interface must be as follows:

$$\geq 45 \text{ Hz}$$

No local mode should be lower than the first fundamental frequencies.

Longitudinal frequencies:

The fundamental frequency in the longitudinal axis of a spacecraft hard-mounted at the interface must be as follows:

$$\geq 90 \text{ Hz}$$

No local mode should be lower than the first fundamental frequencies.

4.2.5 Design Loads

During ground operations and flight, the spacecraft is subjected to various static and dynamic loads. The associated loads at spacecraft-to-adapter interface are defined by Quasi-Static Loads (QSL), that apply at spacecraft center of gravity and that are the most severe combinations of dynamic and static accelerations that can be encountered by the spacecraft at any instant of the mission.

For a spacecraft complying with the stiffness requirements defined in previous paragraph 4.2.3, the limit levels of Quasi-Static Loads, to be taken into account for the design and dimensioning of the spacecraft primary structure, are given in Table 4.2.5 below:

Ground and flight load cases	QSL (g) (Static + Dynamic)		
	Longitudinal		Lateral
	Compression	Tension	
Case 1	- 14.2	+ 10.3	+/- 2.6
Case 2	- 10.0	+ 10.0	+/- 4.0

Table 4.2.5 - Design limit load for Micro Auxiliary Passenger

Notes:

- The factors apply on payload center of gravity,
- The minus sign indicates compression along the longitudinal axis and the plus sign tension,
- Lateral loads may act in any direction simultaneously with longitudinal loads,
- The gravity load is included,
- For the structural design, additional safety factors shall be applied as defined in paragraph 4.3.

4.2.6 Line loads peaking on the spacecraft

The geometrical discontinuities and differences in the local stiffness of the upper part structures (adapters and/or carrying structures) may produce local variations of the uniform line loads distribution.

For the off-the-shelf adapters described in Annex 2, a value of **15%** over the average line loads seen by the spacecraft is to be taken into account.

4.2.7 Line loads peaking induced by the Micro Auxiliary Passenger

The maximum value of the peaking line load induced by the spacecraft is allowed in local areas to be up to **50%** over the maximum line loads induced by the dimensioning loads (deduced from QSL table 4.2.5.).

4.2.8 Handling loads during ground operations

During the encapsulation phase, the spacecraft is lifted and handled with its adapter: for this reason, the spacecraft and its handling equipment must be capable of supporting an additional mass of **15 kg**.

4.2.9 Local loads

On top of the global loads described in the above paragraphs, local loads shall be considered for spacecraft sizing, including payload adapter separation spring forces and flatness effect at spacecraft-to-adapter interface.

4.2.10 Dynamic loads

The secondary structures and flexible elements (e.g., solar panels, antennas, and propellant tanks) must be designed to withstand the dynamic environment with the appropriate safety factors as defined in paragraph 4.3.

4.3 Micro Satellites compatibility verification requirements

During the preparation for launch and during the flight, the spacecraft is exposed to a variety of mechanical, thermal and electromagnetic environments. Refer to Soyuz user's Manual and Vega User's Manual chapter 3 for an extensive description of these environments.

The present Chapter describes the requested demonstrations applicable for Micro Auxiliary Passenger.

4.3.1 Verification Logic

The spacecraft authority shall demonstrate that the spacecraft structure and equipments are capable of withstanding the maximum expected launch vehicle ground and flight environments.

The spacecraft compatibility must be proven by means of adequate tests. The verification logic with respect to the satellite development program approach is shown in Table 4.3.1 below:

S/C development approach	Model	Static	Sine vibration	Random vibration	Acoustic	Shock
With Structural Test Model (STM)	STM	Qual. test	Qual. test	Qual. test	N/A ⁽⁴⁾	Shock test characterization and analysis
	FM1	By heritage from STM ⁽¹⁾	Protoflight test ⁽²⁾	Protoflight Test ⁽²⁾	N/A ⁽⁴⁾	Shock test characterization and analysis or by heritage ⁽¹⁾
	Subsequent FM's ⁽³⁾	By heritage from STM ⁽¹⁾	Acceptance test (optional)	Acceptance test (optional)	N/A ⁽⁴⁾	By heritage and analysis ⁽¹⁾
With ProtoFlight Model (PFM)	PFM = FM1	Qual. test or by heritage ⁽¹⁾	Protoflight test ⁽²⁾	Protoflight Test ⁽²⁾	N/A ⁽⁴⁾	Shock test characterization and analysis or by heritage ⁽¹⁾
	Subsequent FM's ⁽³⁾	By heritage ⁽¹⁾	Acceptance test (optional)	Acceptance test (optional)	N/A ⁽⁴⁾	By heritage and analysis ⁽¹⁾

Table 4.3.1 – Spacecraft verification logic

Notes:

- ⁽¹⁾ If qualification is claimed by heritage, the representativeness of the structural test model (STM) with respect to the actual flight unit must be demonstrated.
- ⁽²⁾ Protoflight approach means qualification levels and acceptance duration/sweep rate.
- ⁽³⁾ Subsequent FM: spacecraft identical to FM1 (same primary structure, major subsystems and appendages).
- ⁽⁴⁾ Acoustic test not required for micro satellites (refer to chapter 4.3.4.5) pending demonstration that the acoustic environment is covered by the random test.

The mechanical environmental test plan for spacecraft qualification and acceptance shall comply with the requirements presented hereafter and shall be reviewed by Arianespace prior to implementation of the first test.

The purpose of ground testing is to screen out unnoticed design flaws and/or inadvertent manufacturing and integration defects or anomalies. It is therefore important that the satellite be mechanically tested in flight-like configuration. In addition, should significant changes affect the tested specimen during subsequent AIT phase prior to spacecraft shipment to CSG, the need to re-perform some mechanical tests must be reassessed. If, despite of notable changes, complementary mechanical testing is not considered necessary by the Customer, this situation should be treated in the frame of a Request For Waiver, which justification shall demonstrate, in particular, the absence of risk for the launcher.

4.3.2 Safety factors

Spacecraft qualification and acceptance test levels are determined by increasing the limit loads by the safety factors given in Table 4.3.2 below. The spacecraft must have positive margins with these safety factors.

SC tests	Qualification ⁽⁴⁾		Protoflight		Acceptance	
	Factors	Duration/Rate	Factors	Duration/Rate	Factors	Duration/Rate
Static (QSL)	1.25	N/A	1.25	N/A	N/A	N/A
Sine vibrations	1.25	0.5 oct./min ⁽²⁾	1.25	1.0 oct./min ⁽²⁾	1.0	1.0 oct./min ⁽²⁾
Random vibrations	2.25 ⁽¹⁾	240 s	2.25 ⁽¹⁾	120 s	1.0 ⁽¹⁾	120 s
Acoustics	+3 dB (or 2)	120 s	+3 dB (or 2)	60 s	1.0	60 s
Shock	+3 dB (or 1.41)	N/A ⁽³⁾	+3 dB (or 1.41)	N/A ⁽³⁾	N/A	

Table 4.3.2 - Test Factors, rate and duration

Notes:

- ⁽¹⁾ Factor by which to multiply the Power Spectral Density.
- ⁽²⁾ See paragraph 4.3.3.2.
- ⁽³⁾ Number of tests to be defined in accordance with methodology for qualification (see paragraph 4.3.3.5.).
- ⁽⁴⁾ If qualification is not demonstrated by test, it is reminded that a safety factor of 2 is requested with respect to the design limit.

The above figures comprise the volume for spacecraft and its adaptor. The allocated volume envelope in the vicinity of the adaptor is described in annex 2 for each of the off-the-shelf adaptors.

2.3.2.2 Usable volume for Micro Auxiliary passenger

The payload usable volume for Micro Auxiliary Passengers is shown below (for S/C and its adaptor):

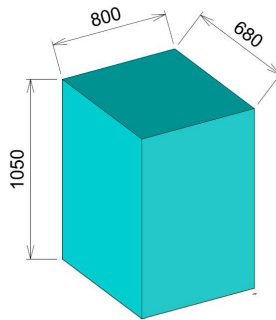


Figure 2.3.2.2a: Micro Aux. Passenger Usable Volume (for S/C and its adaptor)

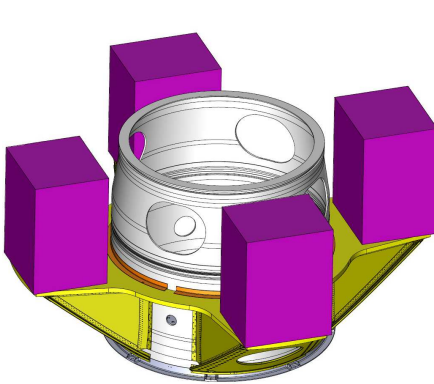


Figure 2.3.2.2b: Micro Aux. Passenger Usable Volume - ASAP-S on Soyuz



Figure 2.3.2.2c: Micro Aux. Passenger Usable Volume - VESPA on VEGA

Note: The above usable volume is only valid with simultaneous separation of an even number of auxiliary passengers, similar in terms of mass.

For spacecraft with protrusions outside these dimensions, please contact Arianespace.

F EOS Aluminum AlSi10Mg Data Sheet



Material data sheet

EOS Aluminium AlSi10Mg

EOS Aluminium AlSi10Mg is an aluminium alloy in fine powder form which has been specially optimised for processing on EOSINT M systems

This document provides information and data for parts built using EOS Aluminium AlSi10Mg powder (EOS art.-no. 9011-0024) on the following system specifications:

- EOSINT M 280
with PSW 3.6 and Original EOS Parameterset AlSi10Mg_Speed 1.0
- EOS M 290 400Watt
with EOSPRINT 1.0 and Original EOS Parameterset AlSi10Mg_Speed 1.0

Description

AlSi10Mg is a typical casting alloy with good casting properties and is typically used for cast parts with thin walls and complex geometry. It offers good strength, hardness and dynamic properties and is therefore also used for parts subject to high loads. Parts in EOS Aluminium AlSi10Mg are ideal for applications which require a combination of good thermal properties and low weight. They can be machined, spark-eroded, welded, micro shot-peened, polished and coated if required.

Conventionally cast components in this type of aluminium alloy are often heat treated to improve the mechanical properties, for example using the T6 cycle of solution annealing, quenching and age hardening. The laser-sintering process is characterized by extremely rapid melting and re-solidification. This produces a metallurgy and corresponding mechanical properties in the as-built condition which is similar to T6 heat-treated cast parts. Therefore such hardening heat treatments are not recommended for laser-sintered parts, but rather a stress-relieving cycle of 2 hours at 300 °C (572 °F). Due to the layerwise building method, the parts have a certain anisotropy, which can be reduced or removed by appropriate heat treatment - see Technical Data for examples.



Material data sheet

Technical data

General process and geometrical data

Typical achievable part accuracy [1] [2]	$\pm 100 \mu\text{m}$
Smallest wall thickness [1] [3]	approx. 0.3 – 0.4 mm approx. 0.012 – 0.016 inch
Surface roughness, as built, cleaned [1] [4]	Ra 6 – 10 μm , Rz 30 – 40 μm Ra 0.24 – 0.39 x 10 ⁻³ inch Rz 1.18 – 1.57 x 10 ⁻³ inch
- after micro shot-peening	Ra 7 – 10 μm , Rz 50 – 60 μm Ra 0.28 – 0.39 x 10 ⁻³ inch Rz 1.97 – 2.36 x 10 ⁻³ inch
Volume rate [5]	7.4 mm ³ /s (26.6 cm ³ /h) 1.6 in ³ /h

[1] These properties were determined on an EOSINT M 270.

[2] Based on users' experience of dimensional accuracy for typical geometries. Part accuracy is subject to appropriate data preparation and post-processing, in accordance with EOS training.

[3] Mechanical stability dependent on the geometry (wall height etc.) and application

[4] Due to the layerwise building, the surface structure depends strongly on the orientation of the surface, for example sloping and curved surfaces exhibit a stair-step effect. The values also depend on the measurement method used. The values quoted here given an indication of what can be expected for horizontal (up-facing) or vertical surfaces.

[5] The volume rate is a measure of the building speed during laser exposure. The overall building speed is dependent on the average volume rate, the time required for coating (depends on the number of layers) and other factors, e.g. DMLS settings.



Material data sheet

Physical and chemical properties of the parts

Material composition	Al (balance) Si (9.0 - 11.0 wt-%) Fe (\leq 0.55 wt-%) Cu (\leq 0.05 wt-%) Mn (\leq 0.45 wt-%) Mg (0.2 - 0.45 wt-%) Ni (\leq 0.05 wt-%) Zn (\leq 0.10 wt-%) Pb (\leq 0.05 wt-%) Sn (\leq 0.05 wt-%) Ti (\leq 0.15 wt-%)
Relative density	approx. 99.85 %
Density	2.67 g/cm ³ 0.096 lb/in ³



Material data sheet

Mechanical properties of the parts

	As built	Heat treated [9]
Tensile strength [6]		
- in horizontal direction (XY)	460 ± 20 MPa 66.7 ± 2.9 ksi	345 ± 10 MPa 50.0 ± 1.5 ksi
- in vertical direction (Z)	460 ± 20 MPa 66.7 ± 2.9 ksi	350 ± 10 MPa 50.8 ± 1.5 ksi
Yield strength (Rp 0.2 %) [6]		
- in horizontal direction (XY)	270 ± 10 MPa 39.2 ± 1.5 ksi	230 ± 15 MPa 33.4 ± 2.2 ksi
- in vertical direction (Z)	240 ± 10 MPa 34.8 ± 1.5 ksi	230 ± 15 MPa 33.4 ± 2.2 ksi
Modulus of elasticity		
- in horizontal direction (XY)	75 ± 10 GPa 10.9 ± 0.7 Msi	70 ± 10 GPa 10.2 ± 0.7 Msi
- in vertical direction (Z)	70 ± 10 GPa 10.2 ± 0.7 Msi	60 ± 10 GPa 8.7 ± 0.7 Msi
Elongation at break [6]		
- in horizontal direction (XY)	(9 ± 2) %	12 ± 2%
- in vertical direction (Z)	(6 ± 2) %	11 ± 2%
Hardness [7]	approx. 119 ± 5 HBW	
Fatigue strength [1] [8]		
- in vertical direction (Z)	approx. 97 ± 7 MPa approx. 14.1 ± 1.0 ksi	

[6] Mechanical strength tested as per ISO 6892-1:2009 (B) annex D, proportional specimens, specimen diameter 5 mm, original gauge length 25 mm (1 inch).

[7] Hardness test in accordance with Brinell (HBW 2.5/62.5) as per DIN EN ISO 6506-1. Note that measured hardness can vary significantly depending on how the specimen has been prepared.

[8] Fatigue test with test frequency of 50 Hz, R = -1, measurement stopped on reaching 5 million cycles without fracture.

[9] Stress relieve: anneal for 2 h at 300 °C (572 °F).

[10] These properties were determined on an EOSINT M 280-400W. Test parts from following machine type EOS M 290-400W correspond with these data.



Material data sheet

Thermal properties of parts

	As built [1]	Heat treated [1] [9]
Thermal conductivity (at 20 °C)		
- in horizontal direction (XY)	approx. 103 ± 5 W/m°C	approx. 173 ± 10 W/m°C
- in vertical direction (Z)	approx. 119 ± 5 W/m°C	approx. 173 ± 10 W/m°C
Specific heat capacity		
- in horizontal direction (XY)	approx. 920 ± 50 J/kg°C	approx. 890 ± 50 J/kg°C
- in vertical direction (Z)	approx. 910 ± 50 J/kg°C	approx. 890 ± 50 J/kg°C

Abbreviations

approx. approximately
wt weight

Notes

The data are valid for the combinations of powder material, machine and parameter sets referred to on page 1, when used in accordance with the relevant Operating Instructions (including Installation Requirements and Maintenance) and Parameter Sheet. Part properties are measured using defined test procedures. Further details of the test procedures used by EOS are available on request.

The data correspond to our knowledge and experience at the time of publication. They do not on their own provide a sufficient basis for designing parts. Neither do they provide any agreement or guarantee about the specific properties of a part or the suitability of a part for a specific application. The producer or the purchaser of a part is responsible for checking the properties and the suitability of a part for a particular application. This also applies regarding any rights of protection as well as laws and regulations. The data are subject to change without notice as part of EOS' continuous development and improvement processes.

EOS®, EOSINT® and DMLS® are registered trademarks of EOS GmbH.

© 2014 EOS GmbH – Electro Optical Systems. All rights reserved.